

# Morphology and Dimension Variations of Copper Sulfide for High-Performance Electrode in Rechargeable Batteries: A Review

Gulnur Kalimuldina, Arailym Nurpeissova, Assyl Adylkhanova, Desmond Adair, Izumi Taniguchi, and Zhumabay Bakenov\*




Cite This: *ACS Appl. Energy Mater.* 2020, 3, 11480–11499

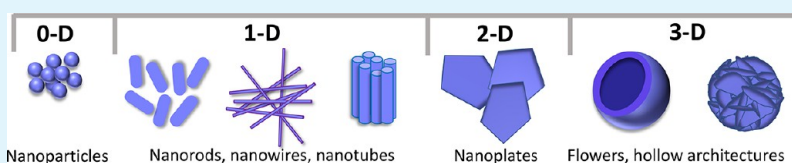


Read Online

ACCESS |

 Metrics & More

 Article Recommendations



**ABSTRACT:** Currently, different metal sulfides (NiS, Co<sub>9</sub>S<sub>8</sub>, FeS<sub>2</sub>, and CuS) have been extensively studied as alternative electrodes for rechargeable batteries that can satisfy the performance requirements for more powerful energy supply and storage technologies for various applications and industries. Among them, copper sulfides have gained significant attention as a promising electrode material in rechargeable metal-ion (Li, Mg, Na, and Al) batteries. A wide range of synthesis routes and methods have been implemented in order to prepare various stoichiometry Cu<sub>x</sub>S (1 ≤ x ≤ 2) micro-/nanostructured materials with excellent electrochemical properties. Since the bulk micro-sized electrode materials have almost reached their performance limits for energy devices, the introduction of nanoscale Cu<sub>x</sub>S composites is now in high demand. This review focuses on the influence of the material morphology and dimensions on their performance in secondary batteries. The structures of Cu<sub>x</sub>S materials from zero-dimensional (0D) to 3D and their preparation are discussed. The primary purpose of this work is to provide an overview of the unique electrochemical and physical properties of particular structure and dimensionality which can promote these materials' application in the energy storage field. Along with this, this work summarizes the information on various synthesis strategies and how they can manage the morphologies of Cu<sub>x</sub>S micro-/nanocomposites. In the current fast technologically advancing society, the development of the most economically profitable and efficient synthesis routes is especially encouraged and required, and this aspect is also commented on in this review.

**KEYWORDS:** copper sulfide, dimensionality, 0D copper sulfide, 1D copper sulfide, 2D copper sulfide, 3D copper sulfide, lithium-ion battery, metal sulfide

## INTRODUCTION

The United Nations Paris Agreement of 2016 declared immediate actions toward reduction of greenhouse gas emissions and mitigation of their negative effects. Environmental concerns initiated and motivated the need for the large-scale implementation of renewable energy sources.<sup>1–3</sup> However, today the intermittent character of renewable energy sources demands efficient energy storage systems to mitigate power fluctuations in order to integrate them into grids. Among various energy storage technologies, rechargeable lithium-ion batteries (LIBs) have proved to be the most promising and applicable for over the past two decades due to their capability to rapidly store and release electricity and to some extent maintain their storage capacity over cycling. Along with the energy generation, the fossil fuel powered transport causes critical air pollution and this motivated rapid development of the market of electrical vehicles (EVs), which is also mainly powered by LIBs. LIBs also dominate the market of

rechargeable batteries for other portable electronic devices and applications.

Microsized bulk composites used in LIBs have already reached their limits in electrochemical performance and cannot satisfy the requirements of the next-generation electrochemical energy devices (EEDs). Therefore, the development of new energy storage materials is urgent for enhanced support of the ever rapidly growing practical needs of our society. Novel advancements in nanoscience are opening new prospects to remarkably improve the performance of materials for super-capacitors, fuel cells, and especially the electrodes for LIBs.

**Received:** July 16, 2020

**Accepted:** October 28, 2020

**Published:** November 16, 2020



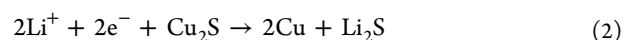
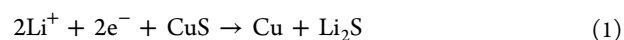
It is acknowledged that the electrodes are an essential part of the battery in relation to their design, structure, and dimensions, since these parameters directly affect the battery power, energy densities, and capacity.<sup>4–6</sup> According to Mei et al.<sup>7</sup> an increase of active mass loading of electrodes helps to increase the energy density, while the power density decreases.<sup>8–10</sup> Also, the decrease of particle size increases power and energy densities.<sup>11–13</sup> Lu et al. investigated different sizes of  $\text{LiMn}_2\text{O}_4$ , and concluded that the reduction of the particle size was responsible for the higher Coulombic efficiency and specific capacity.<sup>8</sup> Since the Li-ion transport in LIBs is rate-limiting in solid materials, i.e., electrode materials, the bigger the particle size, the higher the limiting transport path.<sup>14</sup> Also, it is worth mentioning that recently single crystalline active materials appeared to show superior performance.<sup>15</sup> To investigate the impact of the one-dimensional (1D) and 3D electrodes' thicknesses on the electrochemical and thermal characteristics, Zhao et al. reported that, with an increase of thickness, energy density as well as internal resistance became higher. The investigation stated that in the case of  $\text{LiMn}_2\text{O}_4$  material with an increase of cathode material thickness from 35 to 65  $\mu\text{m}$ , the energy density of 140.99  $\text{Wh kg}^{-1}$  rose to 228.15  $\text{Wh kg}^{-1}$ , while the power density dropped from 313.31  $\text{Wh kg}^{-1}$  to 258.11  $\text{Wh kg}^{-1}$ . This decrease was directly connected to the expansion of discharge time at the same current rate.<sup>10</sup> In addition to these factors, porosity is also one of the important parameters because it affects the kinetics of ion diffusion.<sup>11,16</sup> Meso- and micropores could facilitate access of the electrolyte that improves the transfer of ions between electrodes during charge/discharge processes.

The currently known commercial electrode materials are still in their first generation. The researched electrode materials can be divided into three main categories, depending on their electrochemical reaction mechanisms, as intercalation ( $\text{LiCoO}_2$ ), alloying (Si, Sn), and conversion ( $\text{M}_a\text{X}_b$ , M = transition metal and X = O, S, F, P, N). So far, the different approaches (nanostructuring, surface modifications, carbon coating, and others) have been tried in an attempt to improve the electrochemical properties of the conventional cathode ( $\text{LiCoO}_2$ ) and anode (graphite) materials. Although such battery systems have been widely used in portable electronics, today they are facing critical power limitations for large-scale applications.<sup>17–19</sup> In the case of commercially available cathode  $\text{LiCoO}_2$ , although almost all of the Li can be extracted to give a theoretical capacity of 274  $\text{mAh g}^{-1}$ , only a little over half of the capacity is practically reversible for charge/discharge ( $\leq 4.2$  V vs  $\text{Li/Li}^+$ ). Capacity fading is severe upon extraction of  $>0.7$  Li due to the loss of oxygen, electrolyte decomposition, and the problems of cobalt dissolution in typical electrolytes.<sup>20</sup> Alternatives to  $\text{LiCoO}_2$  are necessary because of its high cost, toxicity, and poor safety, making it unsuitable for large-scale energy storage applications.

On the other hand, the most used graphite anode allows the intercalation of only one Li ion with six carbon atoms, with a resulting stoichiometry of  $\text{LiC}_6$  and thus an equivalent reversible capacity of 372  $\text{mAh g}^{-1}$ .<sup>21</sup> Hence, there also is an urgency to replace graphite anodes with materials with higher capacity, energy, and power density. Today the path leading to metal-ion batteries with improved energy and power densities has, as a major challenge, the selection of suitable electrode materials, which can provide high capacity and easy diffusion of Li ions into the structure, along with good cycling life and freedom from safety concerns.

The need for satisfying the required power demands of EVs and large-scale energy grid systems is pushing researchers' boundaries further in the exploration of many other materials with the most prominent electrochemical properties. In the past few decades metal sulfides ( $\text{NiS}$ ,  $\text{Co}_9\text{S}_8$ ,  $\text{FeS}_2$ ,  $\text{CuS}$ ) have started to be considered as economically viable alternatives due to their unique properties of high conductivity and higher specific capacities in comparison to metal oxide electrode materials.<sup>22–26</sup> Metal sulfides have more valence states and crystal dimensions, making them more attractive due to their electrochemical superiority from the capacity and rate capability points of view.<sup>27</sup> Additionally, metal sulfides are abundant in the Earth crust (for instance, chalcocite); thus, they and their composites are cheap, which means their application can be utilized widely.<sup>28–32</sup>

Among metal sulfides, copper sulfides ( $\text{Cu}_x\text{S}$ ,  $1 \leq x \leq 2$ ) have attracted considerable attention due to their low cost and high theoretical specific capacity (337–560  $\text{mAh g}^{-1}$ ).<sup>26,33</sup> The main feature that makes  $\text{Cu}_x\text{S}$  especially attractive is its high electrical conductivity. It was reported that  $\text{Cu}_2\text{S}$  possessed a high electrical conductivity of about 5–140  $\text{S cm}^{-1}$  and  $\text{CuS}$  of around  $\sim 10^3$   $\text{S cm}^{-1}$ , respectively.<sup>26,34</sup> The general electrochemical reactions of these compounds can be considered as follows with the final products as Cu and  $\text{Li}_2\text{S}$ :<sup>33</sup>



$\text{Cu}_x\text{S}$  materials show two discharge potential plateaus at 2.1 and 1.7 V vs  $\text{Li/Li}^+$  for  $\text{CuS}$ <sup>27,35</sup> and a single potential plateau around 1.7 V for  $\text{Cu}_2\text{S}$ .<sup>34</sup> Over the past ten years, more works have been devoted to investigating the complex reaction mechanism of  $\text{Cu}_x\text{S}$  with metal anodes (Li, Na, Mg, Al) in half-cells and more detailed charge–discharge processes have been reported.<sup>36–39</sup>

Depending on the synthesis procedures of  $\text{Cu}_x\text{S}$ , its electrochemical performance varies because it is strongly related to its structure, including the crystalline nature, particle size, dimensionality, and interface. Therefore, in this work,  $\text{Cu}_x\text{S}$  materials with different morphological structure dimensionalities from 0D to 3D are reviewed, including the synthesis procedures and their structure-related electrochemical performances, when applied as cathode or anode materials in secondary batteries. Copper sulfide has a wide range of nonstoichiometric compounds such as  $\text{Cu}_2\text{S}$ ,  $\text{Cu}_{1.96}\text{S}$ ,  $\text{Cu}_{1.8}\text{S}$ ,  $\text{Cu}_{1.75}\text{S}$ ,  $\text{Cu}_{1.6}\text{S}$ ,  $\text{Cu}_{1.39}\text{S}$ ,  $\text{CuS}$ , and  $\text{CuS}_2$ .<sup>40–42</sup> Among such a large number of  $\text{Cu}_x\text{S}$  phases,  $\text{CuS}$  and  $\text{Cu}_2\text{S}$  are the most investigated. In this review, we aim to accentuate the critical importance of dimensionality on the performance of  $\text{Cu}_x\text{S}$  materials not only in LIBs but also in magnesium-ion batteries (MIBs), sodium-ion batteries (NIBs), and aluminum-ion batteries (AIBs) along with discussions on the synthesis routes.

## ■ DIMENSIONALITY OF NANOSTRUCTURED MATERIALS

Nanostructured materials (NSMs) have attracted great attention due to their unique properties, which were a boon to their application areas in both fundamental and applied sciences because their physical, chemical, and electronic properties show dramatic differences with a change of the dimensionality of the material. Pokropivny and Skorokhod introduced a scheme of classification for NSMs in 2007 such as 0D, 1D, 2D, and 3D, as shown in Figure 1, which was based

Dimensionality classification of nanostructures (  $L < 100 - 500 \text{ nm}$  )Designation: dimensionality of NS  $\rightarrow$   $kDlmn$   $\leftarrow$  dimensionality of elementary units

$$k \geq l, m, n \quad \{k, l, m, n\} = \{0, 1, 2, 3\}$$

Elementary building units :

1. <b>0D</b> Molecules, clusters, fullerenes, rings, metcarbs, thoroids, domens, particles, powders, grains, schwartzons	2. <b>1D</b> nanotubes, fibers, filaments, whiskers, spirals, belts, springs, horns, columns, needles, pillars, helicoids, wires, ribbons	3. <b>2D</b> layers
--	---	---------------------

0D-nanostructures :	4. <b>0D0</b> uniform particles arrays	5. <b>0D00</b> heterogeneous particles arrays, "core-shell" dendrimers, onions
1D-nanostructures :	6. <b>1D0</b> molecular chains, polymers	
7. <b>1D00</b> heteropolymers	8. <b>1D1</b> bundles, ropes, cables, corals	9. <b>1D11</b> heterochains, heterocables, saws, hair, heterobundles, junctions, combs, bows
		10. <b>1D10</b> beads, pea-pods, fullereno-fibers

2D-nanostructures :	11. <b>2D0</b> fullerene films	12. <b>2D1</b> nanostraw, PhC, fibers films
13. <b>2D2</b> tiling, mosaic, layered films	14. <b>2D00</b> heterofilms of heteroparticles, fullereno-powders	15. <b>2D10</b> films of pods, fullereno-fibers
16. <b>2D11</b> films of fibers and nanotubes, PhC-waveguides	17. <b>2D20</b> fullereno-plate films	18. <b>2D21</b> bridges, fiber-layer films
	19. <b>2D22</b> hetero-layers, MOS-structures	20. <b>2D210</b> fullerene-fiber-layer films

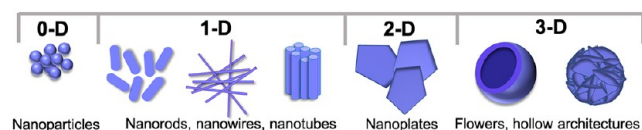
3D-nanostructures :	21. <b>3D0</b> Fullerenes, clathrates, powder skeletons, fog	22. <b>3D1</b> skeletons of fibers, nanotubes	23. <b>3D2</b> layer skeletons buildings, honeycombs, foams	24. <b>3D00</b> sols, colloids, smogs, heteroparticles composites
25. <b>3D10</b> skeletons of fibers-powders	26. <b>3D11</b> skeletons of heterofibers nanotubes	27. <b>3D20</b> intercalates, skeletons of layers and powders	28. <b>3D21</b> Cross-bar-layers, layer-fiber skeletons	
29. <b>3D22</b> heterolayers	30. <b>3D30</b> opals, dispersions, particles, pores, fullerenes in matrix	31. <b>3D31</b> membranes, PhC, fiber composites, waveguides	32. <b>3D32</b> friction pairs, contacts, interfaces, cavities, grain boundaries	
33. <b>3D210</b> composites of layers, fibers and particles in matrix	34. <b>3D310</b> membranes + impurities, powder-fiber composites	35. <b>3D320</b> powder-layers composites	36. <b>3D321</b> layers-fibers-composites in matrix, VCSEL	

Figure 1. Dimensionality classification of nanostructures. Reprinted with permission from ref 44. Copyright 2007 Elsevier.

on the then recently developed composites.<sup>43,44</sup> This figure has been taken as a guide for defining morphology classifications of the subject of studies in this review. Such classification is highly dependent on the electron movement along the dimensions in the NSMs, which generate a series of novel physical and chemical properties that differ from those of conventional bulk materials. For example, rather than electrons in 0D NSMs being entrapped in dimensionless composites, 1D NSMs can move electrons along the  $x$ -axis, and they are less than 100 nm in size. With the increase of dimensionality, the movement of electrons is enhanced, as in 2D, and 3D NSMs where electrons freely move along the  $x$ - $y$ -axes and  $x$ ,  $y$ ,  $z$ -axes, respectively.<sup>31,43-45</sup>

Many techniques have been developed to synthesize and fabricate 0D-3D  $\text{Cu}_x\text{S}$  NSMs with controlled size, shape, dimensionality, and structure. Therefore, the details of the different types of  $\text{Cu}_x\text{S}$  NSMs are discussed here from 0D to 3D, which are synthesized or fabricated by a variety of both simple and complex methods in order to achieve the most attractive electrochemical properties for the next-generation rechargeable metal-ion batteries.<sup>46</sup> Obtained structures of  $\text{Cu}_x\text{S}$  known as nanoparticles, nanorods, nanowires, nanoneedles,<sup>47-49</sup> nanosheets,<sup>50,51</sup> nanothin films,<sup>52</sup> hollow spheres,<sup>53</sup> flower-like structures,<sup>54</sup> and others were taken as the basis of classification by morphological dimensions as shown in Figure 2.





**Figure 2.** Different architectures of  $\text{Cu}_x\text{S}$  developed for rechargeable batteries.

## ZERO-DIMENSIONAL NANOSTRUCTURED MATERIALS

Although a vast amount of different synthesis methods have been developed to fabricate 0D materials, only a few 0D NSMs with  $\text{Cu}_x\text{S}$  have been successful.<sup>46</sup> Today, quantum dot synthesized  $\text{Cu}_x\text{S}$  is widely used in supercapacitors and solar cells, but less in LIBs. This is because for controlled synthesis of 0D and 1D metal sulfide nanostructures, various hard or soft templates such as aluminum oxide pores or surfactant molecules are usually required. These additions to the synthesis procedures increase the reaction complexity and result in potential impurity in the products.<sup>55</sup>

A simple approach is to use commercially available NSMs as recommended by Wu et al.<sup>56</sup> to check properties of  $\text{Cu}_x\text{S}$  in MIBs. Such a system delivers a high reversible capacity of  $175 \text{ mAh g}^{-1}$  at  $50 \text{ mA g}^{-1}$  and a rate capability providing  $90 \text{ mAh g}^{-1}$  at  $1000 \text{ mA g}^{-1}$  as well as a stable cyclability over 350 cycles. These promising properties have been linked to the small-sized copper sulfide particles, which facilitate the solid-state diffusion kinetics.

The work of Kravchyk and co-workers<sup>57</sup> presented a highly reversible electrochemical reaction between Mg and CuS nanoparticles for MIBs as well, with high capacities of  $300 \text{ mAh g}^{-1}$  at room temperature and high cyclic stability over 200 cycles. The current density was  $0.1 \text{ A g}^{-1}$  with a Coulombic efficiency of 99.9%. TEM, XRD, and EDX analysis results are shown in Figure 3. The

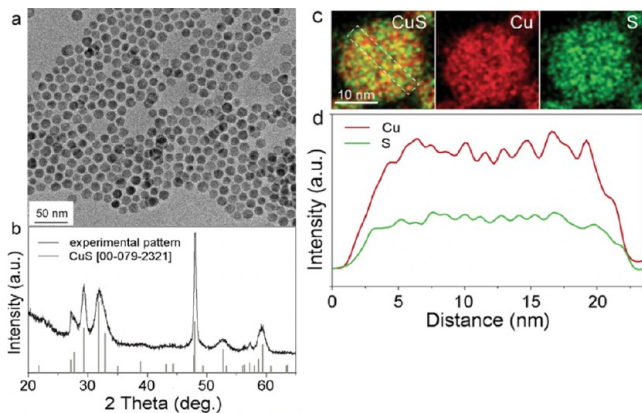


**Figure 3.** TEM image (a) and XRD pattern (b) of CuS NPs. (c) Elemental maps of a single CuS NP using EDX measurements in the HAADF-STEM mode for Cu + S, Cu, and S/ (d) Line scans representing the intensity distribution of Cu (red) and S (green) within the CuS NPs. Reprinted with permission from ref 57. Copyright 2019 The Authors under Creative Commons Attribution 4.0 International License (<http://creativecommons.org/licenses/by/4.0/>), published by Springer Nature.

authors used a mixed solution method with a heat treatment procedure to fabricate the desired nanostructured CuS electrodes. On the other hand, Lui et al.<sup>58</sup> applied a hydrothermal method and subsequent calcination using glucose as a carbon source to obtain a  $\text{Cu}_2\text{S}/\text{C}$  composite material for LIBs. After the heat treatment at  $800^\circ\text{C}$ , the authors succeeded in the formation of interconnected spherical particles. The  $\text{Cu}_2\text{S}/\text{C}$  composites exhibited a discharge capacity of  $300 \text{ mAh g}^{-1}$  after 100 cycles.

## ONE-DIMENSIONAL NANOSTRUCTURED MATERIALS

One-dimensional structures are attractive for researchers because of their enhanced optical, magnetic, and mechanical properties and electrochemical performance.<sup>59</sup> They find applications in nano-thermometers, solar cells, and light-emitting diodes as well as electrodes for LIBs. One-dimensional NSMs vary in diameter from 1 to 100 nm and can be in tube-, rod-, wire- or belt-shaped forms.<sup>60</sup> Plenty of methods to fabricate  $\text{Cu}_x\text{S}$  nanowires/nanorods, namely, the hydrothermal approach, template-assisted route, high-pressure autoclave process, electrodeposition, and thermal evaporation, have been used.<sup>61–66</sup> The 1D composites as nanowires and nanorods are suitable for application in LIBs because their performance can satisfy the requirements for advanced batteries. The advantages of long cyclability and enhanced flexibility lead to the improvement of the contact area between electrolyte and electrode. In the result, increased charge/discharge capacities as well as enhancement of both electrons and Li-ions conductivity were observed.<sup>67–71</sup> Low-dimensional NSMs with large surface areas exhibit superior mechanical, thermal, chemical, and electrical properties to those of bulk materials. The application of 1D NSMs can be possible in a wide range of applications that are not possible with bulk dimensional materials.<sup>59</sup> The reported works dedicated to the preparation of  $\text{Cu}_x\text{S}$  with such beneficial 1D morphologies have delivered excellent electrochemical properties such as cycling stability and higher capacity. The recently reported 1D  $\text{Cu}_x\text{S}$  materials can be grouped into two categories depending on the morphologies: nanowire and nanotube/rod/fiber structures.

**Nanowire Structures.** The advantages of nanowires for energy storage systems are that they have a high contact area between the electrode and electrolyte. Also, it is essential to mention the shortened pathway for Li-ions and electrons transport. These features can improve the electrochemical performance and stability of the electrodes at higher charge–discharge rates.<sup>69,72</sup> The advantage of these properties were demonstrated by Lai et al.<sup>73</sup> who applied a facile solution method to fabricate 1D  $\text{Cu}_2\text{S}$  nanowire arrays. Due to the pure metal sulfide phase, which was provided via this route, it has generated much interest among researchers. Additionally, the material obtained by this method has shown a good cyclability delivering  $250 \text{ mAh g}^{-1}$  for 100 cycles as well as a high Coulombic efficiency (Figure 4). In another work, Feng et al.<sup>49</sup> obtained new copper sulfide

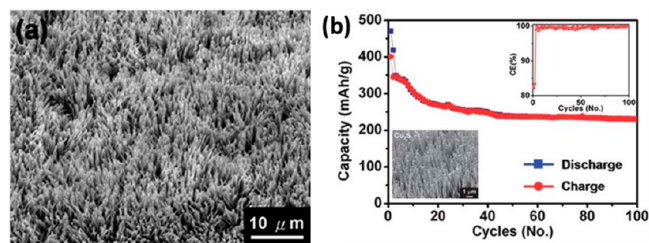


**Figure 4.** SEM images of the as-grown  $\text{Cu}_2\text{S}$  nanostructures. (a) Low-magnification view of a large-area  $\text{Cu}_2\text{S}$  nanowire arrays grown on a copper substrate. (b) Cycle performance of a  $\text{Cu}_2\text{S}$  nanowire array/Li cell operated at a high rate of 2 C. The inset shows the corresponding Coulombic efficiency (CE) of the  $\text{Cu}_2\text{S}$  nanowire array/Li cell. Reprinted with permission from ref 73. Copyright 2010 Royal Society of Chemistry.

nanowire bundles via a template method without any surfactant use, by mixing them in dimethylsulfoxide–ethyl glycol solvents. Because of a specific structure of copper sulfide nanowires, the capacity and cycling stability of LIBs were increased.

**Nanotube/Rod/Fiber Structures.** Similarly to nanofibers, nanotubes/nanorods have also attracted the attention of researchers. They also own a high surface area; and in these materials this advantageous property for enhanced electrochemical activity is strengthened further by the advantages of an interconnected porous network structure with

well-directed 1D conductive paths. Carbon networks have been investigated where nanoscale copper sulfide ( $n\text{-Cu}_2\text{S}$ ) and microscale copper sulfide ( $\mu\text{-Cu}_2\text{S}$ ) were deposited over networks of single-walled carbon nanotubes (SWCNTs) by atomic layer deposition (ALD).<sup>74</sup> The ALD  $\text{Cu}_2\text{S}$  was deposited on networked 1D SWCNTs at 135 °C using an ALD reactor with the morphology shown in SEM images in Figure 5. When the authors compared the effect of different

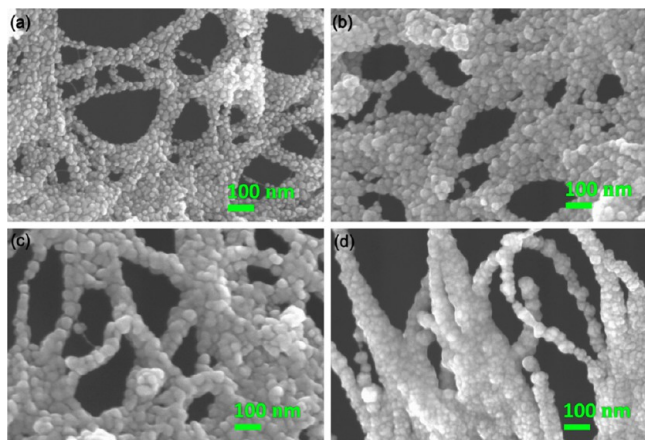


**Figure 5.** SEM images of the ALD-coated SWCNTs following (a) 100, (b) 200, (c) 400, and (d) 600  $\text{Cu}_2\text{S}$  ALD cycles. Reprinted with permission from ref 74. Copyright 2015 Elsevier.

scales of deposited  $\text{Cu}_2\text{S}$  on their electrochemical outcomes, the SWCNT- $\mu\text{-Cu}_2\text{S}$  showed a capacity of 200  $\text{mAh g}^{-1}$  with fast decay upon cycling. The lack of capacity recovery compared to the  $\mu\text{-Cu}_2\text{S}$  suggests that perhaps the material was too dense to allow a rearrangement in the electrode composition. In contrast, the SWCNT- $n\text{-Cu}_2\text{S}$  demonstrated a capacity of about 260  $\text{mAh g}^{-1}$  for 200 cycles. The capacity recovery after a long cycle number in SWCNT- $n\text{-Cu}_2\text{S}$  was linked to increased extensive SWCNT lithiation on the accessible surface.

Zhou et al.<sup>75</sup> published research on 10 nm nanorods by a simple sol-gel method without further thermal operations. According to this work, besides great Coulombic efficiency as well as reversible capacity, the utilized anodes based on these nanorods indicated good cycling up to 250 cycles.

Cai et al.<sup>76</sup> obtained  $\text{Cu}_x\text{S}/\text{Cu}$  nanotubes in poly(ethylene glycol) (PEG). The presynthesized Cu nanowires were converted into nanotubes via a mass diffusion. The work demonstrated that  $\text{Cu}_x\text{S}/\text{Cu}$  nanocomposites show a stable cyclability with a fifth-cycle discharge capacity of 282  $\text{mAh g}^{-1}$ . It was concluded that the PEG capping helped to reduce the dissolution of polysulfides.

A tubular carbon matrix was used to impregnate sulfur through heat treatment in a sealed vessel.<sup>77</sup> The electrode was coated on a Cu foil, and a  $\text{Cu}_2\text{S}/\text{tubular}$  mesoporous carbon composite was produced via electrochemical charge-discharge-assisted processes.  $\text{Cu}_2\text{S}$  with in situ preparation showed the highly reversible and very stable capacity of 270  $\text{mAh g}^{-1}$  for 300 cycles at 1 C rate. Li et al.<sup>45</sup> synthesized 1D  $\text{Cu}_x\text{S}$  nanorods via the hydrothermal route without using any surfactants. Both of the electrodes based on CuS and  $\text{Cu}_2\text{S}$  composites demonstrated high cyclability as well as rate capability, with initial capacities found as 370 and 260  $\text{mAh g}^{-1}$ , respectively. Due to a facile synthesis and excellent electrochemical performance, these nanorods are promising anodes for LIBs. Yang et al.<sup>78</sup> presented a CuS cathode material via a surfactant-assisted hydrothermal route. It was highlighted that participation of sulfurating reagents and synthesis temperature directly impacted the morphology of copper sulfide nanorods.

Chen and coauthors<sup>79</sup> prepared a new combination of  $\text{Cu}_2\text{S}$  with an N and S dual-doped carbon matrix ( $\text{Cu}_2\text{S}@\text{NSCm}$ ) by a simple in situ polymerization process and subsequent carbonization for both LIB and NIB. The morphological study showed that short nanorods

have the length of  $\sim 200$  nm and a diameter of  $\sim 40$  nm. The first charge/discharge capacities of  $\text{Cu}_2\text{S}@\text{NSCm}$  in LIB were 558.4  $\text{mAh g}^{-1}$  and 894.8  $\text{mAh g}^{-1}$ , respectively, in the 0.01–3.0 V range vs  $\text{Li}/\text{Li}^+$ . As for the NIBs, the first discharge capacity of 949.8  $\text{mAh g}^{-1}$  dropped to 182.3  $\text{mAh g}^{-1}$  after 50 cycles in a potential range of 0.01–3.0 V vs  $\text{Na}/\text{Na}^+$  at 100  $\text{mA g}^{-1}$ .

## ■ TWO-DIMENSIONAL NANOSTRUCTURED MATERIALS

Recently, 2D materials are gaining even more interest due to their unique structure and surface area resulting in enhanced and pronounced physical and chemical properties. Furthermore, 2D materials exhibit special shape-dependent features; therefore, they can be used as the major components for building blocks in nano-devices.<sup>80,81</sup> Another benefit of utilizing 2D materials is that this type of composite can easily interact and combine with 0D, 1D, and 2D materials.<sup>80,82,83</sup> Thus, the mentioned features of these materials can be utilized for secondary batteries in all fields (anodes, cathodes, and separators). Due to the large surface area, porous structure, and good chemical stability, 2D materials can be employed as host materials for copper sulfide cathodes.<sup>84–86</sup> Besides being used as host materials, 2D materials promote the reaction kinetics to lethargic kinetics and eventually increase the electrode output. Over the past years, numerous types of 2D materials such as graphene, borophenes, transition metal oxides/sulfides/nitrides/carbides/phosphides, metal-organic frameworks (MOFs), polymers, and 2D hybrid materials have been applied for LIB compartment improvements.<sup>85</sup> Furthermore, 2D nanomaterials can be hybridized to the van der Waals solids of hetero-nanosheets which have properties (synergistic or compensating) that cannot be easily achieved by general 2D nanomaterials.<sup>46</sup> In this section, various kinds of 2D  $\text{Cu}_x\text{S}$  materials known as nanoplates, nanobranches, and nanosheets prepared for LIBs and NIBs have been demonstrated.

**Graphene-Based  $\text{Cu}_x\text{S}$  Structures.** It has been reported that most of the metal sulfides suffer from fast reversible capacity fading due to the large volume variation during the lithiation and delithiation processes and dissolution of lithium polysulfides in the electrolyte.<sup>87</sup> The use of a carbon matrix is considered as one of the effective approaches to solving these issues, as it acts as a buffer to mitigate the volume expansion and an electrically conductive media.<sup>88,89</sup> So far, the investigation papers on the improvement of  $\text{Cu}_x\text{S}$  properties through adopting graphene, graphene oxide (GO), or reduced graphene oxide (rGO) matrix have been reported on using  $\text{Cu}_x\text{S}$  as the anode material for LIBs.

Hydrothermal treatment is one of the most available and simple methods to obtain 2D NSMs. For example, Tao et al.<sup>90</sup> fabricated  $\text{CuS}/\text{graphene}$  composite by the one-pot hydrothermal method using thiourea both as the sulfur source and reducing agent. To see the effect of the addition of graphene, the authors compared charge-discharge profiles of CuS and  $\text{CuS}/\text{graphene}$ . For the CuS electrode, the first discharge and charge capacities were 525 and 311  $\text{mAh g}^{-1}$ , respectively. However, the first discharge and charge capacities of the  $\text{CuS}/\text{graphene}$  composite were significantly improved up to 827 and 484  $\text{mAh g}^{-1}$ , respectively. Another work with rGO as the framework for  $\text{Cu}_x\text{S}$  was reported by Ren et al.<sup>50</sup>  $\text{CuS}$  nanoparticles were homogeneously dispersed on the surfaces of rGO nanosheets via a hydrothermal method as well. The obtained “double-sandwich-like” structure led to improvement in the electrochemical performance of electrodes. Authors linked the reported achievements to the reduced transport path length for both  $\text{Li}^+$  ions and electrons due to the rGO double-sandwich-like structure, as it improves lithium insertion/desertion from the liquid electrolyte or anode structure. The discharge capacity showed 648.1  $\text{mAh g}^{-1}$  at the second cycle and later increased at the 100th cycle to 710.7  $\text{mAh g}^{-1}$ .

Ding et al.<sup>91</sup> reported the combination of hydrothermal and freeze-drying steps to prepare hierarchical CuS. The freeze-drying technique gave uniform mixing of the CuS microparticles with flexible graphene layers as can be observed in Figure 6. The BET analysis of specific surface area of  $\text{CuS}/\text{graphene}$  composites showed 177.34  $\text{m}^2 \text{g}^{-1}$ ,



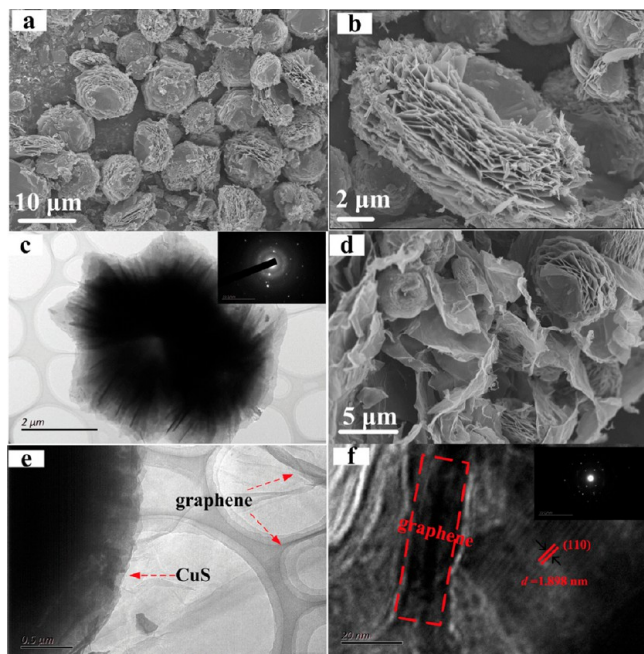


**Figure 6.** Typical morphologies and structures of CuS and CuS/graphene composite: (a, b) SEM images and (c) TEM image of CuS. The inset of panel c is the SAED pattern of CuS. (d) SEM, (e) TEM, and (f) HRTEM images of the CuS/graphene composite. The inset of panel f is a typical SAED pattern of the CuS/graphene composite. Reprinted with permission from ref 91. Copyright 2017 Elsevier.

which was much higher than that of bare CuS ( $32.29 \text{ m}^2 \text{ g}^{-1}$ ). Accordingly, the CuS/graphene electrode delivered higher initial discharge and charge capacities of 1318.9 and  $854.6 \text{ mAh g}^{-1}$ , respectively. More complex composite materials as graphene/polyaniline/CuS nanocomposite (GR/PANI/CuS NC) was fabricated by a combination of hydrothermal and in situ polymerization methods.<sup>92</sup> The cycle performance showed outstanding properties of GR/PANI/CuS NC with a reversible specific capacity of  $1255 \text{ mAh g}^{-1}$  after 250 cycles.

Microwave-assisted hydrothermal synthesis is a fast route to fabricate desirable morphologies of NSMs with stable stoichiometric compositions. For instance, Yuan et al.<sup>93</sup> synthesized a CuS/rGO nanoflower composite by an ultrafast microwave-assisted hydrothermal method using  $\text{Cu}(\text{NO}_3)_2$ , thiourea, and GO powders as the precursor. The rate capability tests of the CuS/rGO electrodes exhibited capacities of 543, 484, 473, 458, and  $453 \text{ mAh g}^{-1}$  at the current densities of 100, 200, 500, 800, and  $1000 \text{ mA g}^{-1}$ , respectively. One-pot microwave irradiation was also used to prepare CuS/graphene electrodes.<sup>94</sup> CuS spherical particles with a diameter of about 800 nm were formed on the graphene sheets. The electrochemical tests showed that pristine CuS had a capacity of  $379 \text{ mAh g}^{-1}$  after 100 cycles at  $0.2 \text{ A g}^{-1}$ , while CuS-G exhibited improvements delivering the capacity of  $497 \text{ mAh g}^{-1}$  after 100 cycles.

Implementation of  $\text{Cu}_x\text{S}$  electrodes in NIBs has also been gaining in application over the past few years. For instance, microwave treatments have been used by Li and coauthors<sup>95</sup> to obtain CuS with a different mass percentage of rGO (20.8%, 26.7%, and 34.0%). Through the modification of a cutoff potential, there was an attempt to improve the electrochemical properties of CuS/rGO with diethylene glycol dimethyl ether (NaFS/DGM) electrolyte. At the potential range of 0.4–2.6 V vs  $\text{Na}/\text{Na}^+$  a discharge capacity of  $392.9 \text{ mAh g}^{-1}$  after 50 cycles was delivered for 34.0% of the rGO in the CuS.

CuS nanowires were successfully obtained on the rGO by a simple one-pot general solution method in a DMSO-EG solvent.<sup>49</sup> Compared to pure CuS nanowires, this type of composite showed excellent energy storage performance and long-term stability. For

instance, its reversible capacity was  $620 \text{ mAh g}^{-1}$  at 0.5 C after 100 cycles. In another work, Zhang et al.<sup>96</sup> have similarly synthesized  $\text{Cu}_x\text{S}$  microspheres wrapped in rGO with a two-step method. Initially,  $\text{Cu}_x\text{S}/\text{rGO}$  was prepared by mixing the solution, and then  $\text{Cu}_x\text{S}/\text{rGO}$  was obtained by adding sulfur. XRD showed the mix of the phases as CuS and  $\text{Cu}_2\text{S}$  in their electrodes with a capacity of  $320 \text{ mAh g}^{-1}$  for 100 cycles at a constant current of  $200 \text{ mA g}^{-1}$ . Contrary, wet chemical methods could be considered a much simpler way to prepare hierarchical CuS/rGO composites.<sup>97</sup> The SEM image of the hierarchical CuS-rGO demonstrated that the diameter of the samples was about  $2.5 \mu\text{m}$  with the hierarchical CuS microballs confined by graphene. The initial specific discharge capacity of the hierarchical CuS-rGO was  $810 \text{ mAh g}^{-1}$ . However, after 50 cycles, the capacity value of the hierarchical CuS-rGO dropped and remained at  $450 \text{ mAh g}^{-1}$ . Such excellent results of application of the graphene-based media in  $\text{Cu}_x\text{S}$  electrodes could be attributed to the synergistic effects between  $\text{Cu}_x\text{S}$  and graphene in the composite electrode.

**Carbon-Coated/-Added  $\text{Cu}_x\text{S}$  Structures.** Coating is one of the most effective approaches used to boost the electrochemical performance of different materials. For instance, carbon coating is widely used to enhance Li–S battery properties.<sup>98</sup> The improvements have been ascribed to the physical and chemical stabilities of the coating layer, which is beneficial in maintaining the morphology of well-designed nanostructures and reduces the loss of active mass during long-term cycling.<sup>88</sup> As for the  $\text{Cu}_x\text{S}$  electrodes, carbon coating/addition not only enhances the electronic conductivity but also reduces the lithium polysulfides dissolution in the electrolyte and their diffusion/shuttle.<sup>99</sup>

Zhang et al.<sup>100</sup> fabricated carbon-coated  $\text{C}@\text{Cu}_{1.96}\text{S}$  nanosheets by annealing MOF and commercially available sulfur powder. MOF is known as an effective precursor for fabrication of carbon materials and metal oxides with novel nanoarchitectures or enhanced porosities. The electrochemical performance of the obtained  $\text{C}/\text{Cu}_{1.96}\text{S}$  was improved, showing a high reversible capacity of  $240 \text{ mAh g}^{-1}$  during the 50th cycle with capacity retention of 94%. Liu et al.<sup>89</sup> also applied a one-pot microwave-assisted solvothermal approach highly used in preparation of 1D NSMs to fabricate copper sulfide and carbon hybrid nanotubes. The obtained hybrid material as CuS-CNTs exhibited  $339 \text{ mAh g}^{-1}$  at  $0.5 \text{ A g}^{-1}$ . It was reported that unique hybrid nanotubes were one of the main facilitators of high reversible capacity, cycling stability, and rate capability.

Nanoplates and nanodisks are known for their enhanced access by electrolyte and accordingly improved  $\text{Li}^+$  diffusion. The method of chemical dealloying was used to prepare CuS nanowire-on-nanoplate by Wang and co-workers.<sup>48</sup> According to this work, the nanoplate matrix was uniformly covered with nanowires with 4–7 nm width and 40–60 nm lengths. The CuS nanowire-on-nanoplate structured electrode exhibited a capacity of  $425 \text{ mAh g}^{-1}$  after 100 cycles.

In another approach, copper sulfide nanodisks (CuS-NDs) were fabricated using a simple low-temperature reaction and applied as the anode materials for NIBs with acid-treated single-walled carbon nanotubes (a-SWCNTs), which acted as a paper-like nanohybrid. The nanohybrids had a high reversible capacity of  $610 \text{ mAh g}^{-1}$  and high rate current rates of  $0.1\text{--}3 \text{ A g}^{-1}$  during the conversion reaction which formed  $\text{Na}_2\text{S}$  and Cu metal in reverse.<sup>101</sup> CuS nanoplates were also prepared for NIBs by using a solvothermal method from a transparent microemulsion consisting of CTAB, *n*-pentanol, and copper nitrate trihydrate. Carbon disulfide was added to the microemulsion before transferring it into the Teflon-sealed autoclave. During the electrochemical tests of CuS with Na, such nanoplates experienced severe capacity deterioration of up to  $80 \text{ mAh g}^{-1}$  at 0.2 C, and CuS after the first 13 cycles. However, with the increase of the cycle number, the capacity gradually recovered to  $570 \text{ mAh g}^{-1}$ . The work tried to understand the reasons for the capacity recovery using a series of analysis of ex situ TEM of the cycled CuS nanoplates. According to the studies, sodium insertion–extraction stress changes the morphology of the nanoplates into small grainy parts with 1–20 nm sizes (Figure 7).<sup>102</sup>

**Thin Film  $\text{Cu}_x\text{S}$  Structures.** The advantage of thin film is that it does not need additional carbon sources to enhance conductivity or

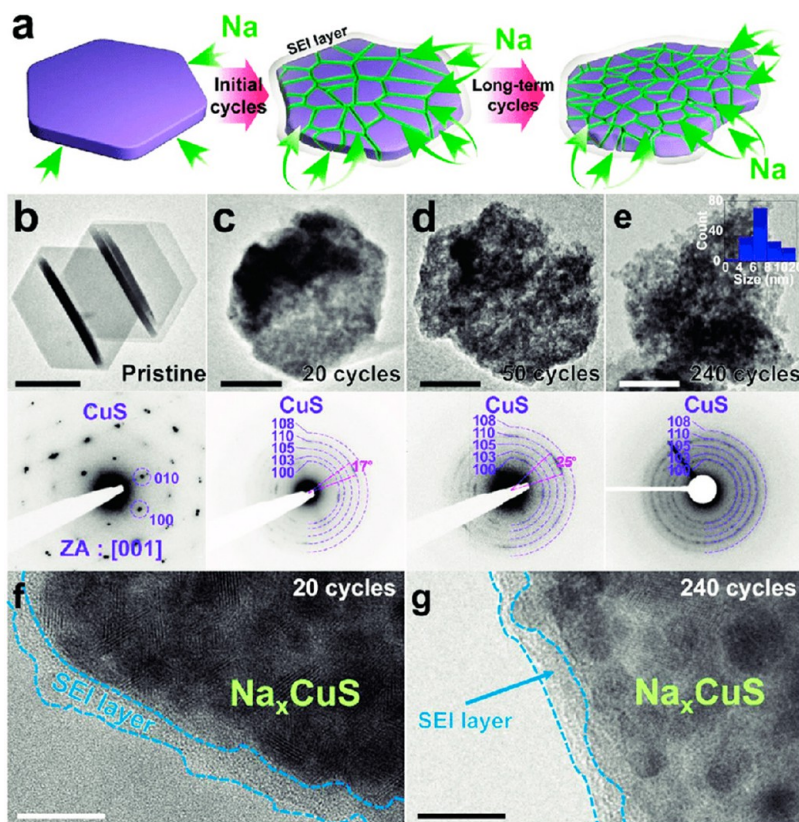


**Figure 7.** Ex situ observation of CuS nanoplates disintegration. (a) Schematic model demonstrating the disintegration in CuS nanoplates. Low-magnification TEM images and corresponding SAED patterns of (b) pristine CuS (scale bar, 200 nm) and desodiated CuS nanoplates (scale bar, 100 nm) after (c) 20 cycles, (d) 50 cycles, and (e) 240 cycles at 0.2 C. Inset graph in panel d shows the size distribution of CuS nanograins. TEM images of the SEI layers on the surface of  $\text{Na}_x\text{CuS}$  after (f) 20 cycles (scale bar, 20 nm) and (g) 240 cycles (scale bar, 10 nm). Reprinted with permission from ref 102. Copyright 2019 The Authors under CC BY-ND 2.0 (<https://creativecommons.org/licenses/by-nd/2.0/>), published by Wiley-VCH.

polymer binders due to the extreme thinness of the electrode. However, only in a few works on the synthesis of CuS thin films the electrodes application in secondary batteries can be found. One of them is by the Tarascon group<sup>103</sup> on the preparation of CuS thin films by electrodeposition by cyclic voltammetry (CV). Here the electrolytic bath consisted of  $\text{Cu}(\text{TFSI})_2$  and sulfur powder in the ionic liquid  $[\text{EMIm}]\text{TFSI}$ . In Figure 8, SEM images of the resulting CuS flakes with 50 nm thickness are shown. This CuS structure exhibited the first discharge capacity of  $545 \text{ mAh g}^{-1}$  at C/20, which is close to 97.4% of the theoretical capacity.

A widely used microwave-assisted method mentioned above was also implemented to fabricate CuS thin films by Xiao et al.<sup>104</sup> Initially, circular Cu metal foil with a diameter of 12 mm was dispersed in sulfur dissolved *N*-methyl-2-pyrrolidinone (NMP) solution and then microwave irradiated. The morphology of the reaction product changed from CuS nanobuds to nanosheets with the increase of the microwave irradiation temperature. The binder-free Cu-supported CuS nanosheets demonstrated a reversible capacity of  $490 \text{ mAh g}^{-1}$  for 100 cycles at 1 C rate. On the other hand, a less stable cyclability was shown by nanobuds-shaped CuS with capacity of about  $271 \text{ mAh g}^{-1}$  after 100 cycles at the same current density.

Another approach as hydrothermal treatment allowed direct growth of  $\text{Cu}_2\text{S}$  film on a Cu foil as demonstrated by Ni and coauthors.<sup>52</sup> The obtained  $2 \mu\text{m}$  thickness  $\text{Cu}_2\text{S}$  thin film revealed a capacity of  $0.32 \text{ mAh cm}^{-2}$  in the 200th cycle at a current density of  $0.1 \text{ mA cm}^{-2}$ . Mazor et al.<sup>105</sup> also investigated CuS thin film application in microbatteries. The electrodeposition from an electrolytic bath of 1,2-propanediol propylene glycol, ethylenediaminetetraacetic acid–disodium–copper ( $\text{CuNa}_2\text{EDTA}$ ), and elemental sulfur was used in this case. Planar  $\text{Li}/\text{CuS}_x$  cells showed reversible capacities of  $120\text{--}150 \mu\text{Ah cm}^{-2}$  and a peak power of  $18.5 \text{ mW cm}^{-2}$ .

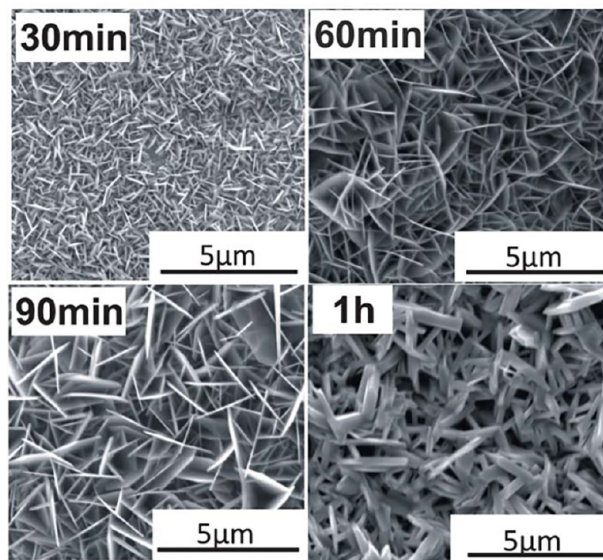


**Figure 8.** SEM images of CuS films prepared with different reaction times. Reprinted with permission from ref 103. Copyright 2012 Royal Society of Chemistry.

### ■ THREE-DIMENSIONAL MICRO-/NANOSTRUCTURED MATERIALS

Due to the unique high surface area, large surface-to-volume ratio, and more favorable structural stability in comparison with their 0D, 1D,



and 2D counterparts, 3D architectures have been investigated with much interest. As was mentioned before, the behavior of nanomaterials depends on their shape, size, morphology, and dimensions. Therefore 3D materials, as for 2D materials, due to their controllable structure, high surface area, great absorption abilities, and better electron conductivity (better transportation of electrons and ions) are very promising as electrodes for energy storage devices. Because the main criteria for selection of the electrode materials for rechargeable batteries are their energy and power densities, advanced 3D nanoarchitecture materials have been developed using two core principles: increasing the electrochemically active surface area and shortening the ionic transport pathway. To do so, the surface area should be increased by constructing hierarchical structures or hollow structures while the thickness should stay as thin as possible to provide a short ion diffusion length. Different types of 3D  $\text{Cu}_x\text{S}$  nanomaterials were developed utilizing different approaches from hard-template to template-free synthesis methods and investigated in rechargeable metal-ion batteries.

**Hierarchical Structures.** Hierarchical architectures can be defined as assemblages of molecular units, their aggregates of primary nanoparticles embedded within other particles or agglomerates that may, in turn, be part of even larger units of increasing levels of the organization.<sup>106</sup> The controllable synthesis of 3D hierarchical  $\text{Cu}_x\text{S}$  nanostructures with highly active building blocks generates high specific surface areas and facilitates fast migration of ions, enhancing performances of energy storage devices. The growth of hierarchical  $\text{Cu}_x\text{S}$  architectures can be achieved by utilizing simple solution chemical route methods, including solvothermal, hydrothermal, and so on. Chen et al.<sup>107</sup> obtained novel stick-like copper sulfide hierarchical structures via a hydrothermal approach by using  $\beta$ -cyclodextrin as the ligand which generated different morphologies. The 3  $\mu\text{m}$  in diameter sticks were composed of tens to hundreds of well-arranged and self-assembled hexagonal-phase covellite  $\text{CuS}$  nanoplates with a thickness of about 25 nm, as seen in Figure 9b. Electrochemical measurements vs  $\text{Li}^+/\text{Li}^0$  demonstrated good cycle stability with a capacity of 93  $\text{mAh g}^{-1}$  after 30 cycles.

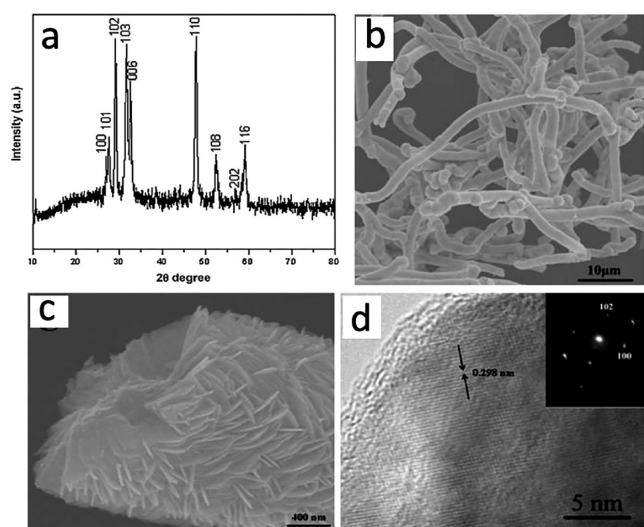


**Figure 9.** XRD pattern (a), SEM images (b, c), and HRTEM image (d) of the products prepared at 120 °C for 12 h. The inset in panel d shows the SAED pattern. Reprinted with permission from ref 107. Copyright 2013 Elsevier.

Using the same method but different Cu and S sources and a surfactant, nanoflakes, microspheres, microflowers, and nanowires of  $\text{CuS}$  were prepared and investigated as cathode materials for LIBs. Phases of all four products examined by XRD were indexed as an orthorhombic  $\text{CuS}$ . When tested in coin cells, the initial specific discharge capacities for  $\text{CuS}$  nanoflakes, microspheres, microflowers, and nanowires were 200, 258, 225, and 262  $\text{mAh g}^{-1}$ , respectively.

Because of their nano-/microparticle size and compact structure, microspheres showed the best capacity retention whereas the nanowire electrode showed the best rate capability (58  $\text{mAh g}^{-1}$  at 1 C). This is due to the high accessibility of the electrolyte, short lithium diffusion length, and porous nanowire structure.<sup>108</sup> Although the stick architectures have been reported, they are not as common as hierarchical flower-like architectures for copper sulfides. So far, a solvothermal method was adopted to design sphere-like  $\text{CuS}$  hierarchical structures without any template and surfactants. In a typical synthesis procedure, Cu and S sources were introduced to different solutions with subsequent heat treatment.<sup>109,110</sup> Microspheres with the morphology consisting of tens to hundreds of well-arranged and self-assembled 20 nm thin cubic phase  $\text{CuS}$  nanoplates were obtained from a mixture of sulfur and ethanol. They delivered an initial capacity of around 600  $\text{mAh g}^{-1}$ .<sup>109</sup> Wang and co-workers<sup>38</sup> also described very similar structures assembled from hexagonal  $\text{CuS}$  nanoplates with high crystallinity. The microspheres as the cathode material for AIBs, built from nanoplates with a mean edge length of about 1  $\mu\text{m}$  and an average thickness of about 13 nm (Figure 10c,d), exhibited a capacity of about 90  $\text{mAh g}^{-1}$  with nearly 100% Coulombic efficiency after 100 cycles at a current density of 20  $\text{mA g}^{-1}$ .

A one-step solvothermal method was practiced to synthesize unique  $\text{CuS-CTAB}$  (cetyltrimethylammonium bromide) microspheres, with tunable interlayer space and micropores, by embedding CTAB directly into hexagonal  $\text{CuS}$  layers. The 3  $\mu\text{m}$   $\text{CuS-CTAB}$  microspheres consist of  $\text{CuS-CTAB}$  nanowalls with an increasing interlayer spacing from 0.8 to 1.2 nm. The main benefit of using CTAB surfactant is that it can absorb polysulfide anions to prevent the dissolution of polysulfide as well as to buffer the volume change. As a result, the  $\text{CuS-CTAB}$  electrodes had a reversible capacity of 684.6  $\text{mAh g}^{-1}$  and possessed a long-term cyclability of 1000 cycles. The excellent rate and ultralong cycling stability performance were attributed to the inserted cationic CTAB molecules which overcome the main problems of  $\text{CuS}$  electrodes in conversion reaction and limiting polysulfide shuttling.<sup>111</sup>

Once again, the one-step solvothermal method, assisted by a polymer template was used to synthesize the  $\text{Cu}_9\text{S}_5\text{-AHP}$  (amino-ended hyperbranched polyamide) structure. Here AHP was used as a template and an additive agent. AHP and salt of copper were dissolved in a methanol solution, after which copper cations connected with AHP amino groups, forming specific hierarchical  $\text{Cu}_9\text{S}_5$  microspheres under thermal conditions. To investigate the influence of AHP on the formation of microspheres, the mole ratio of AHP was varied ( $\text{Cu}_9\text{S}_5\text{-AHP-}x$ ,  $x = 0.5, 1.5, 2.0$ ). A 3D microflower-like architecture with a uniform size of  $\sim 500$  nm was obtained with  $\text{Cu}_9\text{S}_5\text{-AHP} = 1.5$ , which consisted of assembled rhombohedral  $\text{Cu}_9\text{S}_5$  nanoplates with uniform thickness. The Na-storage properties of as-prepared  $\text{Cu}_9\text{S}_5\text{-AHP-1.5}$  were tested. As a result, the cell delivers an outstanding cycling stability, achieving reversible capacity of 386.0  $\text{mAh g}^{-1}$  after 200 cycles with a capacity retention rate of 90%. A polymer framework, where  $\text{Cu}_9\text{S}_5$  nanograins were uniformly dispersed, enhances the diffusion of Na ions and alleviates the nanoparticle aggregation, hence improving the electrochemical performance.<sup>112</sup>

In another work, 3D  $\text{CuS}$  nanoplates for NIBs were synthesized by Park et al.<sup>113</sup> The obtained  $\text{CuS}$  nanoplates showed a unique structure with two thin interweaving plates having an average diameter of  $\sim 300$  nm and thickness of  $\sim 30$  nm as shown in Figure 11. Such morphology is assumed to provide a large surface area and access to Na ions during the charge–discharge processes. The cycling was performed in a potential range of 0.05–2.6 V, and after 80 cycles the capacity and Coulombic efficiency were maintained close to  $\sim 560$   $\text{mAh g}^{-1}$  and  $\sim 100\%$ , respectively for 50 cycles. However, the initial capacity of 680  $\text{mAh g}^{-1}$  deteriorated significantly to 80  $\text{mAh g}^{-1}$ .

An and colleagues<sup>114</sup> synthesized a copper sulfide microflower composite by a straightforward dealloying method. The investigation showed that this type of anode could enhance the diffusion of the Na ions and also provided more space to accommodate volume changes. For the electrochemical properties, high discharge capacity (325.6



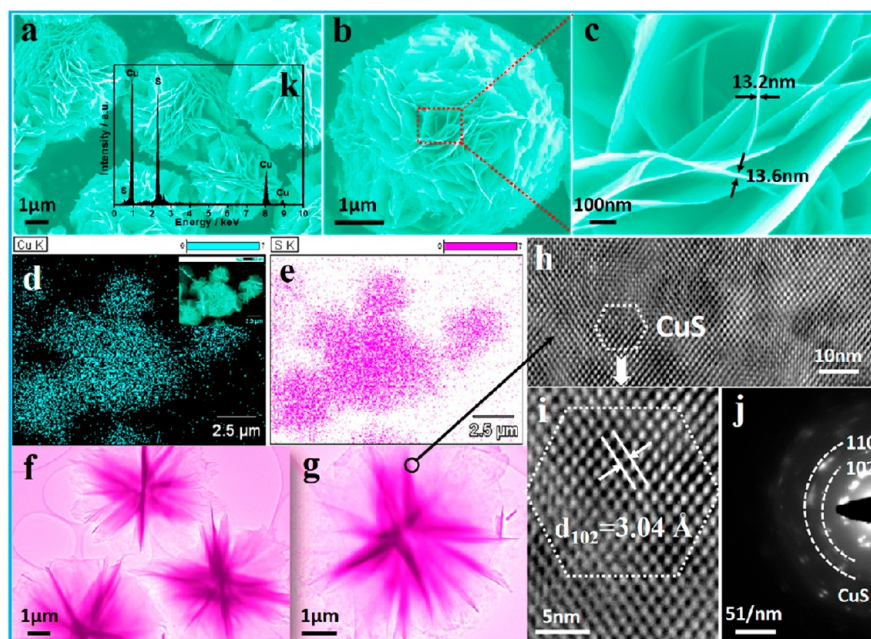


**Figure 10.** Morphologies and compositions of the as-prepared 3D hierarchical nanostructured CuS microspheres. (a–c) FE-SEM images at different magnifications, (d, e) elemental mapping images of Cu and S, (f, g) TEM images, (h–j) HRTEM images and corresponding SAED pattern, and (k) representative EDS spectrum of the as-prepared CuS. Reprinted with permission from ref 38. Copyright 2017 American Chemical Society.

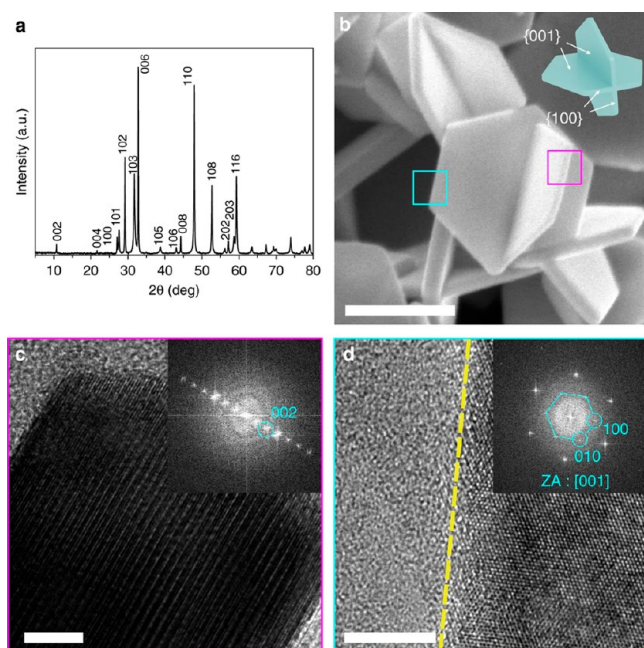


**Figure 11.** Three-dimensional structure of as-synthesized CuS nanoplates. (a) XRD patterns of nanoplates, (b) SEM image and the corresponding schematics of three-dimensional CuS nanoplates (scale bar, 200 nm). HR-TEM images of (c) side plane (scale bar, 5 nm) and (d) basal plane with [001] zone axis (ZA) showing that each plane corresponds to {100} and {001}, respectively (scale bar, 5 nm). Reprinted with permission from ref 113. Copyright 2018 The Authors under Creative Commons Attribution 4.0 International License (<https://creativecommons.org/licenses/by/4.0/>), published by Springer Nature.

mAh g<sup>-1</sup> at 0.1 A g<sup>-1</sup>), outstanding rate capability, and excellent cycling stability even after 5000 cycles with negligible capacity degradation were exhibited. Flower-like 10 μm diameter microspheres

of copper sulfides (CuSs) were synthesized via a facile hydrothermal method by Shi and co-workers.<sup>115</sup> The unique hierarchical structure of CuS was composed of approximately 50 nm thickness nanosheets. The constructed Na/CuS cell delivered an initial discharge capacity of 348.6 mAh g<sup>-1</sup> which decreased to 41.8 mAh g<sup>-1</sup> after 100 cycles. On the other hand, Li<sup>116</sup> fabricated copper sulfide microspheres via a simple microwave method without any additional additives/surfactants. It should be noted that the discharge capacity remained at 162 mAh g<sup>-1</sup> even after 200 cycles, showing capacity retention of 95.8%, demonstrating a high cycling stability.

Spray Pyrolysis is another widely used method for the preparation of spherical nanoparticles. Kalimuldina and Taniguchi<sup>34,117–119</sup> demonstrated a simple synthesis method of Cu<sub>2</sub>S and spherical particles with a geometric mean diameter of 0.45 μm with the precursors being Cu(NO<sub>3</sub>)<sub>2</sub> and thiourea. Cu<sub>2</sub>S on a Cu foil current collector exhibited a stable capacity of 250 mAh g<sup>-1</sup> at 1 C and 220 mAh g<sup>-1</sup> at 30 C, respectively.<sup>34</sup> Another work of these authors on CuS showed promising results with 440 mAh g<sup>-1</sup> for 200 cycles at 1 C and an excellent rate capability with a high capacity of 340 mAh g<sup>-1</sup> at 10 C.<sup>87</sup>

**Hybrid Cu<sub>x</sub>S Three-Dimensional Structures.** Along with the above hierarchical Cu<sub>x</sub>S architectures, modified Cu<sub>x</sub>S structures have been reported. Decorating the structure with carbon and GO sheets suppresses severe volume change and prevents the escape of polysulfides from the active material, thus enhancing the electrochemical performance. Qin et al.<sup>120</sup> prepared a CuS@Sisal fiber carbon (SFC) composite as anode material for lithium-ion batteries via a facile hydrothermal approach, which consisted of homogeneous dispersion of copper sulfide nanoparticles on a Sisal fiber carbon surface. In comparison with general SFC, CuS@SFC exhibited better electrochemical properties; for instance, a discharge capacity was 903 mAh g<sup>-1</sup>, while the reversible capacity after 30 cycles was 303 mAh g<sup>-1</sup>.

In another work, Jing and colleagues<sup>121</sup> reported an easy and straightforward synthesis of a new anode material based on copper sulfide and S, N, and C sources. The anode was fabricated via a facile one-step calcination of copper pyrrithione (C<sub>5</sub>H<sub>4</sub>NOS)<sub>2</sub>Cu. The obtained black powder consisted of 29 nm nanoparticles well-wrapped by a carbon layer with non-uniform thickness, which could clearly be observed via transmission electron microscopy. In terms of electro-

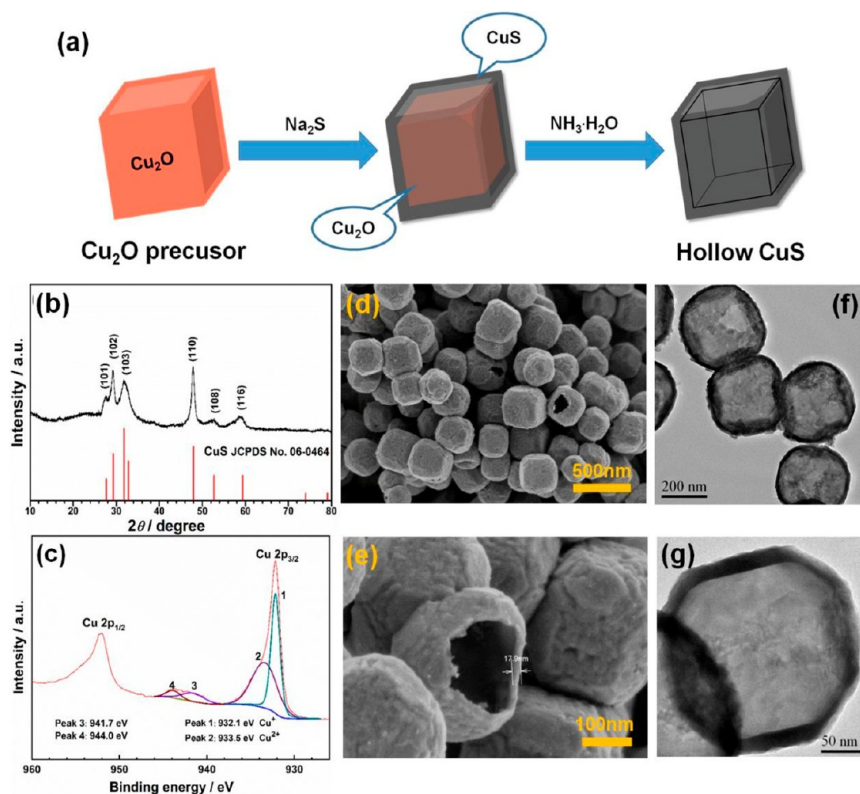


**Figure 12.** (a) Schematic illustration for the fabrication process of hollow CuS nanocubes. (b) XRD pattern, (c) XPS spectra, (d, e) SEM images, and (f, g) TEM images of CuS-I. Reprinted with permission from ref 39. Copyright 2019 Royal Society of Chemistry.

chemical performance, the  $\text{Cu}_9\text{S}_5/\text{NSC}$  electrode delivered a high reversible capacity of  $412.0 \text{ mAh g}^{-1}$  at  $100 \text{ mAh g}^{-1}$  as well as an excellent cycling stability even after 200 cycles.

Zhang and co-workers<sup>96</sup> fabricated novel copper sulfide microspheres wrapped with rGO for LIBs via a two-step solvothermal reaction. The electrochemical performance of this anode was promising with the high cycling stability and rate capability. Moreover, the synergistic effect between  $\text{Cu}_x\text{S}$  and rGO nanosheets was responsible for accommodating volume changes as well as for preventing the dissolution of polysulfides. In comparison with the previous works, their copper sulfide composite maintained a reversible capacity of  $320 \text{ mA g}^{-1}$  even after 100 cycles at a 1 C rate.

A new method of obtaining a  $\text{Cu}_x\text{S}$  cathode is considered as environmentally friendly and economically feasible.<sup>64</sup> It is based on controllable thermal sulfurization, which leads to the formation of  $\text{Cu}_x\text{S}$  different phases. Desired phases of copper sulfide can be prepared at higher temperatures via using MOF of Cu-BTC  $\{[\text{Cu}_3(\text{C}_9\text{H}_3\text{O}_6)_2(\text{H}_2\text{O})_3]_n\}$  (HKUST-1) and sulfur placed in a quartz box. Moreover, the electrochemical properties of the composite prepared by this method were found to be excellent, where the specific capacity reached  $220 \text{ mAh g}^{-1}$  even after 200 cycles.

**Hollow Structures.** In comparison with all the structures of copper sulfides mentioned above, 3D hollow architectures attracted much interest due to their superior energy storage abilities. It was suggested that this is due to the large surface area (outer and inner surfaces), low material density, and capability to cope with volume expansion during cycling in comparison to the nonhollow counterparts. Additionally, the thin walls of hollow structures efficiently facilitate the diffusion of electrons and ions, thus enhancing the electrochemical kinetics. Design and fabrication of hollow architectures have been mainly conducted by the hard and soft template, and one-pot template-free synthesis methods.<sup>122</sup> However, these methods are costly and complex and require toxic reagents.<sup>123</sup> Despite these challenges, a significant amount of a variety of hollow structures were extensively studied in order to be used in rechargeable batteries.

Hard-template synthesis is the most effective strategy available for fabricating the shape-controlled hollow structures, which can maximally inherit the shapes and configurations of the templates. Thus, hollow CuS nanocubes were fabricated using the most common hard-template  $\text{Cu}_2\text{O}$ , as illustrated in Figure 12. Hollow nanocube structures with different side lengths, wall thickness and BET surface areas were obtained by varying the amount of  $\text{Na}_2\text{S}$  solution and investigated as MIB cathodes.<sup>39</sup> The  $200 \text{ nm}$  structure with a wall thickness of  $18 \text{ nm}$  produced using a dilute solution of  $\text{Na}_2\text{S}$ , exhibits high capacity ( $200 \text{ mAh g}^{-1}$ ), remarkable rate capability, and superior long-term cyclability. Such hollow architectures greatly enhance the diffusion of Mg-ions and electrons transport; thus, the electrodes exhibit an improved conductivity.

The same procedure was adopted to synthesize CuS nanoboxes of about  $500 \text{ nm}$  edge length with approximately  $10\text{--}20 \text{ nm}$  wall thickness. CuS/Li cell demonstrates superior cycling stability for 1300 cycles at 2 C without noticeable capacity fading, and even at the high rate of 20 C, a discharge capacity of  $371 \text{ mAh g}^{-1}$  and 86% capacity retention are obtained. This makes the CuS nanoboxes a promising electrode material for Li metal battery applications. Fast  $\text{Li}^+$  diffusion was found to be responsible for the superior cycle stability and rate capability of the CuS nanobox electrode.<sup>124</sup>

Along with this, digenite  $\text{Cu}_{1.8}\text{S}$  with a hollow octahedral structure was synthesized and its Na storage properties were investigated. The top-down approach by a combination of a post calcination and a phase transition from the  $\text{Cu}_{1.6}\text{S}$  phase to  $\text{Cu}_{1.8}\text{S}$  was adopted. TEM analysis shows the individual  $\text{Cu}_{1.8}\text{S}$  particle with dimensions of about  $\sim 800 \text{ nm}$  in length and  $\sim 650 \text{ nm}$  in width, and a wall thickness of  $\sim 100 \text{ nm}$ . The contrast difference between the core and the shell clearly confirms the hollow characteristic. When employed as an anode in NIBs,  $\text{Cu}_{1.8}\text{S}$  hollow octahedra exhibited good reversibility and a capacity of  $403 \text{ mAh g}^{-1}$  (93% of the theoretical one) in  $1.0 \text{ M NaCF}_3\text{SO}_3/\text{dyglomera}$ . The  $\text{Cu}_{1.8}\text{S}$  hollow octahedra electrode shows a reversible charge capacity of  $\sim 250 \text{ mAh g}^{-1}$  and high Coulombic efficiency of  $\sim 100\%$  over 1000 cycles at the high rate of 2 C in a



potential range of 0.5–2.2 V vs Na/Na<sup>+</sup> without irreversible phase transformation and structural collapse.<sup>125</sup>

The same hard-template method was adapted to the elegant multistep templating strategy to rationally synthesize hierarchical double-shelled nanoboxes with the CoS<sub>2</sub> nanosheet-constructed outer shell supported on the CuS inner shell. With these structural and compositional advantages, these hierarchical CuS@CoS<sub>2</sub> nanoboxes manifest boosted electrochemical properties of high reversible capacity (625 mAh g<sup>-1</sup>), outstanding rate performance (304 mAh g<sup>-1</sup> at 5 A g<sup>-1</sup>), and excellent cycling stability (79% capacity retention after 500 cycles).<sup>126</sup>

As mentioned before, hard-template synthesis is very complex and requires costly reagents. Therefore Zhao et al.<sup>53</sup> have presented a facile bubble template (soft template) synthesis method to obtain copper sulfide with sub-micrometer hollow and porous spheres (Figure 13). The work briefly compared the initial discharge output of

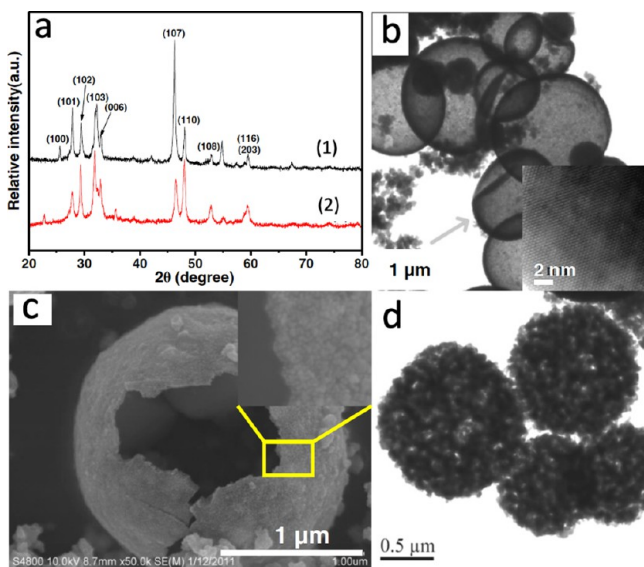


**Figure 13.** (A) X-ray diffraction patterns (a) CuS hollow spheres and (b) porous spheres. (B) TEM image of the as-prepared CuS hollow spheres. The inset is the corresponding HRTEM image. (C) SEM image of the as-prepared CuS hollow spheres. The higher magnification image is also inserted. (D) TEM image of the obtained CuS porous spheres. Reprinted with permission from ref 53. Copyright 2012 Elsevier.

porous and hollow spherical sub-micrometer particles. During the first discharge process, the hollow sphere samples show an initial discharge capacity of 480 mAh g<sup>-1</sup>, while porous sphere samples exhibit a specific capacity of 276 mAh g<sup>-1</sup>.

An alternative strategy was adopted by Nagarathinam and co-workers<sup>54</sup> to obtain 3D hollow spheres and flower-like spheres of copper sulfide via a hydrothermal reaction by utilizing a novel 2D polymer as a precursor. Because of the cavities that could provide extra electrochemically active sites and a large electrolyte–electrode interface for fast metal-ion diffusion, the hollow sphere particles showed outstanding performances.

Yu et al.<sup>37</sup> demonstrated the fabrication of a novel hierarchically structured CuS with a pine-needle-like morphology self-assembled (Figure 14) from hollow nanotubes with a simple reflux template free cosolvent assisted method. When employed as an anode for NIBs, the unique architecture was able to deliver a reversible capacity of 522 mAh g<sup>-1</sup> at 0.1 A g<sup>-1</sup>, superior rate capability with a discharge capacity of 317 mAh g<sup>-1</sup> at 20 A g<sup>-1</sup>, and a long-term cycling stability with a capacity retention of 90% at 2 A g<sup>-1</sup> over 600 cycles. Such a unique interconnected hollow structure of CuS is favorable for penetration of the electrolyte and charge transportation, contributing to achieving excellent electrochemical performance.

Similarly, CuS dandelion-like clusters were synthesized by a simple colloidal approach.<sup>127</sup> The authors were able to obtain such a structure by varying the solvent. When employed as an electrode in LIBs, electrochemical data indicated improved performance delivering 420 mAh g<sup>-1</sup> at 1.12 A g<sup>-1</sup>, and at 0.56 A g<sup>-1</sup>, the capacity was as high as 500 mAh g<sup>-1</sup> with good capacity retention.

**Hybridized Cu<sub>x</sub>S Hollow 3D Structures.** In addition to the development of unique 3D architectures, considerable efforts have been invested in the rational design of nanohybrid Cu<sub>x</sub>S with various carbonaceous materials, transition metal oxides, and metal sulfides, to improve the electrochemical performance by taking advantage of their high electrical conductivity and reliability.<sup>36</sup> This strategy is the common approach to effectively increasing the electronic conductivity and accommodating the volume expansion caused by CuS during cycling. A template-engaged strategy was adopted to synthesize nitrogen-doped carbon-coated Cu<sub>9</sub>S<sub>5</sub> bullet-like hollow particles starting from bullet-like ZnO particles. An initial capacity of 385 mAh g<sup>-1</sup> with a high initial Coulombic efficiency of about 94% was observed when the electrode was tested electrochemically. The unique structure and composition of bullet hollow structured particles pictured in Figure 15 manifest excellent sodium storage properties with a superior rate capability and ultrastable cycling performance over 500 cycles at 0.3 A g<sup>-1</sup>.<sup>128</sup>

Additionally, Wang et al.<sup>99</sup> presented a report on a self-templating thermolysis method to obtain uniform and monodisperse copper

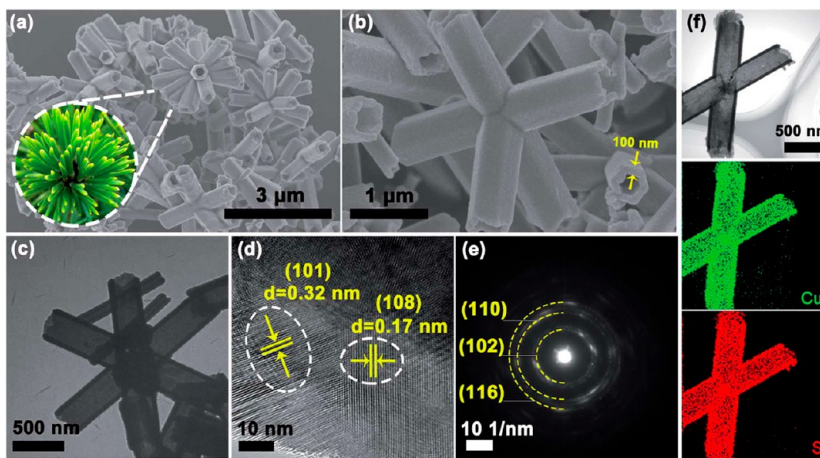


**Figure 14.** Morphology and microstructure of PNL-CuS: (a, b) FESEM images. (c) TEM image. (d) HRTEM image. (e) SAED pattern of PNL-CuS and (f) elemental mapping of Cu and S. The inset of panel a is the image of pine needles. Reprinted with permission from ref 37. Copyright 2019 Royal Society of Chemistry.

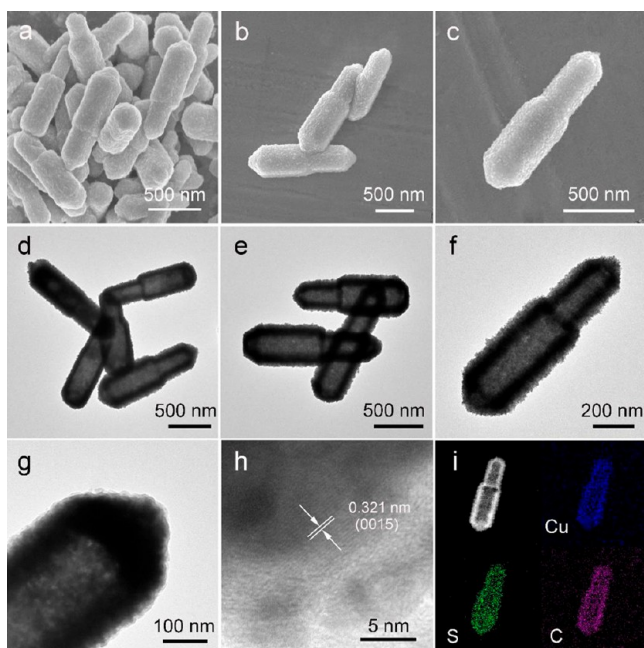


**Figure 15.** (a–c) FESEM images, (d–g) TEM images, (h) HRTEM image of the  $\text{Cu}_9\text{S}_5@NC$  hollow bullets, and (i) elemental mapping images of an individual  $\text{Cu}_9\text{S}_5@NC$  hollow bullet. Reprinted with permission from ref 128. Copyright 2019 Wiley-VCH.

sulfide hollow spheres coated with various shells. The shell-coating materials were chosen, carbon,  $\text{TiO}_2$ , and  $\text{MoS}_2$ , after which the electrodes were assembled to investigate their electrochemical characteristics, and particularly, they were focused on the  $\text{Cu}_{2-x}\text{S}@C$  composite. In comparison to uncoated and coated with  $\text{TiO}_2$ ,  $\text{MoS}_2$  copper sulfide, the  $\text{Cu}_{2-x}\text{S}@C$  anode exhibited an initial discharge capacity of  $353 \text{ mAh g}^{-1}$  and impressive long-term cycling performance which can be related to the synergistic effect of the carbon shell and the hollow interior. While the carbonaceous layer suppresses the loss of active material, substantially improving the cyclability, the internal hollow space can effectively buffer the volume change due to conversion reaction.

**Self-Standing 3D  $\text{Cu}_x\text{S}$  Structures.** To circumvent the low electronic conductivity and morphology destruction during conversion reactions, previously mentioned works mainly focused on alleviating the structural degradation via nanostructure design and improving the electronic conductivity of  $\text{Cu}_x\text{S}$  materials. Nonetheless, prepared nanocomposite powders require the addition of conductive agents, binders, and current collectors to make compact and conductive electrodes. Self-standing electrodes are the best approach to avoid the use of additional components while increasing the active material mass. Different types of self-standing  $\text{Cu}_x\text{S}$  have been proposed and implemented for rechargeable batteries.<sup>129,130</sup> For example, Tang and colleagues<sup>129</sup> reported on the synthesis of  $\text{CuS}@Cu$  freestanding electrodes via electrochemical corrosion. In a typical process, commercially available Cu foam was introduced to the solution of thiourea and hydrogen peroxide with subsequent autoclaving. The electrode was able to deliver charge/discharge capacities of  $845/834 \text{ mAh g}^{-1}$ , respectively, after 500 cycles, which is attributed to the continuous network of Cu structure. This provides faster diffusion of ions and helps to suppress the volume change. Another work was devoted to the sulfuration of Cu foam via a low-temperature dry thermal sulfuration method.<sup>130</sup> The as-prepared  $\text{Cu}_2\text{S}/Cu$  cathode performed excellently when cycled over 100 cycles at different current densities. The excellent rate capability and cycle stability of  $\text{Cu}_2\text{S}/Cu$  cathode is attributed to the unique structure of the electrode. Recently the facile approach of soaking Cu foam in a DMSO/S solution was used to prepare  $\text{Cu}_{1.8}\text{S}$  and  $\text{Cu}_{1.96}\text{S}$  electrodes

for LIBs. The cell demonstrated the stable capacity of about  $250 \text{ mAh g}^{-1}$  in the case of  $\text{Cu}_{1.8}\text{S}$ .<sup>131</sup>

## ■ FULL-CELLS WITH $\text{Cu}_x\text{S}$ ELECTRODES

Although above we discussed the effect of dimensionality on the electrochemical performance of  $\text{Cu}_x\text{S}$  electrodes in half-cells mainly, the full capability of application of such batteries should be tested further in the full-cell configurations. So far, only a few works can be found demonstrating the practical application of  $\text{Cu}_x\text{S}$  electrodes in full-cells. One-dimensional structured copper sulfides in the form of  $\text{Na}_3\text{V}_2(\text{PO}_4)_3/C$  (NVP/C)|| $\text{CuS}$  nanowires@N-doped carbon (NWs@NC) full-cells were successfully assembled by employing NVP/C and the Na activated CuS NWs@NC as the cathode and anode materials, respectively.<sup>132</sup> The obtained full-cells demonstrated a high discharge capacity of  $406 \text{ mAh g}^{-1}$  with a high 96.0% Coulombic efficiency. Moreover, after 200 cycles, the full-cell retained a reversible capacity of  $220 \text{ mAh g}^{-1}$ , with the average Coulombic efficiency of 97.3%. Zhao and colleagues' outstanding results indicate that CuS NWs@NC could be considered a promising anode material for practical application in SIBs.

Another application of commercial CuS in full-cells has been demonstrated for SIBs by combining with NASICON type materials as  $\text{Na}_3\text{V}_2(-\text{PO}_4)_2\text{F}_3/\text{Na}_3\text{V}_2(\text{PO}_4)_3$  (NVPF/NVP) (Fe 8.9%) electrode.<sup>133</sup> The full-cell exhibits a capacity of  $101 \text{ mAh g}^{-1}$  (based on the cathode material mass) and an energy density of  $162.2 \text{ Wh kg}^{-1}$  (based on the mass of both electrode materials) with 2.09 V at 1 C. In this work, the suggested full-cell configuration delivered superior cycling stability even at a high current density of 10C with a capacity of  $71.4 \text{ mAh g}^{-1}$  after 1200 cycles. Both materials used in the full-cell are low in cost and abundant, defining that the suggested full SIB with CuS is quite suitable to match LIBs in supporting energy storage systems and high-power devices.

CuS nanospheres were obtained by a simple solvothermal method that was implemented for the Mg storage in the full-cell system.<sup>134</sup> The challenges of such configurations are that just a negligible electrochemical activity could be obtained at room temperature ( $25^\circ\text{C}$ ), impeding the CuS cathode application in MIBs. The authors used 0.5 M  $\text{Mg}(\text{ClO}_4)_2$  dissolved in acetonitrile ( $\text{Mg}(\text{ClO}_4)_2/\text{AN}$ ) as an electrolyte, AC clothes were utilized as an anode. At  $50^\circ\text{C}$ , CuS cathode in full MIBs at  $20 \text{ mA g}^{-1}$  exhibits a high capacity of  $148 \text{ mAh g}^{-1}$ . Moreover, with the increased current rate to  $50 \text{ mA g}^{-1}$  for 30 cycles, the CuS cathode still exhibits a capacity of  $119 \text{ mAh g}^{-1}$ . The reported results were one of the best for CuS cathodes in an application for MIBs. Once again, this proves that the CuS electrode with different dimensionalities and morphologies has a great potential to gain the deserved spot as a part of the next-generation batteries with high reversible capacity and excellent cycling performance.

Table 1 summarizes the electrochemical properties of  $\text{Cu}_x\text{S}$  materials within the 0D–3D morphologies for LIB, NIB, MIB, and AIB. The collected data analysis demonstrates that  $\text{Cu}_x\text{S}$  is a unique material that can act both as a cathode and an anode material. For instance, as an anode compartment in the metal battery, the potential range was tested between 0.01 and 3.0 V, while for a cathode it was investigated between 1.0 and 3.0 V, respectively. The different dimensionality of  $\text{Cu}_x\text{S}$  defined according to the particular synthesis method delivers different charge/discharge capacities and stability of the cycle life. This helps to determine the method that can facilitate the specific



**Table 1. Comparison of Electrochemical Properties, Surface Area/Mass Loading, Coulombic Efficiency (CE) of 0D to 3D Cu<sub>x</sub>S Micro-/Nanostructured Materials for Secondary Batteries**

material	electrode/battery	synthesis method	electrochemical performance					ref	
			capacity, mAh g <sup>-1</sup> (cycle)	potential range, V	current rate	surface area, m <sup>2</sup> g <sup>-1</sup>	mass loading, mg cm <sup>-2</sup>		CE at first cycle, %
Cu <sub>2</sub> S nanoparticles	cathode/MIB	commercial powder	125 (1st) and 200 (30th)	0.3–2.2	50 mA g <sup>-1</sup>	10,8675	3.5	~90	56
	cathode/MIB	mixed solution	512 (1st)	0.9–1.2	0.1 A g <sup>-1</sup>	n/a		99.9 (2nd)	57
			300 (100th)	2.8–4.4					
Cu <sub>2</sub> S/C nanoparticles	anode/LIB	hydrothermal	322 (1st) and 300 (100th)	0.01–3.0	100 mA g <sup>-1</sup>	n/a	n/a	83	58
			1D Electrodes						
Cu <sub>2</sub> S nanowires	cathode/LIB	general solution	470 (1st)	0.01–2.5	2 C	n/a	n/a	82	73
			230 (100th)	0.05–3.0	2 C				
Cu <sub>2</sub> S nanowire bundles	cathode/LIB	template- and surfactant-free	832 (1st) and 505 (50th)	0.05–2.7	0.2 C	n/a	n/a	n/a	49
			C nanotube- Cu <sub>2</sub> S						
SWCNT- <i>r</i> -Cu <sub>2</sub> S:	cathode/LIB	atomic layer deposition	744 (1st)	0.01–3.0	100 mA g <sup>-1</sup>	n/a	n/a	35	74
			200 (200th)					80 (2nd)	
SWCNT- <i>n</i> -Cu <sub>2</sub> S:	cathode/LIB	atomic layer deposition	451 (1st)	0.01–3.0	100 mA g <sup>-1</sup>	n/a	n/a	34	
			260 (200th)					80 (2nd)	
Cu <sub>2</sub> S nanorods	anode/LIB	sol-gel	775 (1st) and 390 (250th)	0.01–3.0	0.2 C	n/a	n/a	69.8	75
			779 (1st) and 465 (50th)	0.001–3.0	200 mA g <sup>-1</sup>	n/a	n/a	74.6	76
Cu <sub>2</sub> S/tubular carbon	cathode/LIB	in situ electrochemical	270 (300th)	1.0–3.0	1 C	n/a	0.7–1.0	92	77
			Cu <sub>2</sub> S and CuS nanorods						
Cu <sub>2</sub> S:	anode/LIB	hydrothermal	350 (1st) and 313 (100th)	0.8–3.2	100 mA g <sup>-1</sup>	n/a	n/a	93	45
			547 (1st) and 472 (100th)					94	
CuS:	anode/LIB	hydrothermal	100 (1st) and 87.4 (50th)	1.8–2.6	30 mA g <sup>-1</sup>	n/a	n/a	92	77
			CuS nanorods						
Cu <sub>2</sub> S@NSCm	anode/LIB, /NIB	in situ polymerization	894.8 (1st) and 164.8 (150th)	0.01–3.0	200 mA g <sup>-1</sup>	n/a	n/a	62.4	79
			949.8 (1st) and 182.3 (50th)	0.01–3.0	200 mA g <sup>-1</sup>	n/a	n/a	n/a	
LIB:	anode/LIB, /NIB	in situ polymerization	2D Electrodes						
			827 (1st) and 296 (25th)	0.01–3.0	50 mA g <sup>-1</sup>	n/a	n/a	n/a	90
CuS/graphene	anode/LIB	one-pot hydrothermal	851 (1st) and 710.7 (100th)	0.001–3.0	0.2 C	n/a	1.67	66.2	50
			1318.9 (1st) and 147 (100th)	0–3	50 mA g <sup>-1</sup>	177.34	1.0	64.8	91
GR/PANI/CuS NC	anode/LIB	hydrothermal and in situ polymerization	1655 (1st) and 1255 (250th)	0.01–3.0	0.1 A g <sup>-1</sup>	57.8	n/a	99 (250th)	92
			422 (1st)	1.0–3.0	100 mA g <sup>-1</sup>	n/a	1.5	99 (70th)	93
CuS/rGO	anode/LIB	microwave-assisted hydrothermal	390 (70th)	0.01–3	100 mA g <sup>-1</sup>				
			570 (1st) and 497 (100th)	1.0–3.0	0.2 A g <sup>-1</sup>	n/a	2.0–2.5	100 (1000th)	94
CuS/graphene	anode/LIB	one-pot microwave	62 (1st) and 392.9 (50th)	0.4–2.6	100 mA g <sup>-1</sup>	33.66	1.61	94	95
			908 (1st) and 620 (100th)	0.02–3.00	0.5 C	n/a	n/a	n/a	n/a
CuS nanowires/rGO	anode/LIB	one-pot and template-free solution	460 (1st) and 230 (100th)	0.05–3.0	200 mA g <sup>-1</sup>	n/a	1.0–2.0	n/a	96
			810 (1st) and 451 (50th)	0.005–3.0	100 mA g <sup>-1</sup>	n/a	1.8	n/a	n/a
CuS/rGO	anode/LIB	wet chemical	353 (1st) and 240 (50th)	0.8–3.0	0.2 C	n/a	4	n/a	98
			710 (1st) and 425 (100th)	1.0–3.0	0.2 C	n/a	1.0–1.1	87.4	48
C@Cu <sub>1.96</sub> S nanosheets	cathode/LIB	direct sulfuration							
			chemical dealloying						
CuS nanowire-on-nanoplate	anode/LIB								

Table 1. continued

material	electrode/battery	synthesis method	electrochemical performance					ref	
			capacity, mAh g <sup>-1</sup> (cycle)	potential range, V	current rate	surface area, m <sup>2</sup> g <sup>-1</sup>	mass loading, mg cm <sup>-2</sup>		CE at first cycle, %
CuS nanodisks CuS nanoplates CuS-CNTs	anode/SIB	low-temperature reaction	560 (1st) and 400 (40th)	0.01–2.7	100 mA g <sup>-1</sup>	n/a	2.0	~100 (500th)	101
	cathode/SIB	conversion reaction	246 (1st) and 570 (300th)	0.05–2.6	0.2 C	n/a	n/a	n/a	102
	anode/LIB	one-pot microwave-assisted solvothermal	639 (1st) and 483 (150th)	0.01–3.0	0.2 A g <sup>-1</sup>	n/a	n/a	n/a	89
CuS thin films	cathode/LIB	electrodeposition	545 (1st) and 350 (20th)	1.5–2.5	C/20	n/a	n/a	n/a	103
	cathode/LIB	microwave	720 (1st)	1.0–3.0	0.1 C	n/a	n/a	100 (11th)	104
Cu <sub>2</sub> S thin films	cathode/LIB	hydrothermal	490 (100th)	1.0–3.0	1 C	n/a	n/a	85.5	52
	cathode/LIB	hydrothermal	0.34 (500th)	0.02–3.5	0.1 mA cm <sup>-2</sup>	n/a	n/a	99 (30th)	107
stick-like CuS hierarchical structures CuS	cathode/LIB	hydrothermal	94 (1st) and 93 (30th)	1.8–2.6	0.2 C	n/a	n/a	n/a	108
	cathode/LIB	hydrothermal	200 (50th)	1.8–2.6	0.1 C	58.2	n/a	n/a	108
nanoflakes: microspheres: microflowers: nanowires:	cathode/LIB	hydrothermal	258 (50th)	1.8–2.6	0.1 C	23.9	n/a	n/a	108
	cathode/LIB	hydrothermal	225 (50th)	1.8–2.6	0.1 C	36.7	n/a	n/a	108
CuS with hierarchical structures CuS microspheres	anode/LIB	solvothermal	262 (50th)	0.01–3.0	100 mA g <sup>-1</sup>	82.3	2.6–3.4	n/a	109
	cathode/AIB	solvothermal	582 (1st) and 80 (10th)	0.01–3.0	20 mA g <sup>-1</sup>	n/a	n/a	13.8	110
CuS-CTAB microspheres	anode/SIB	one-step solvothermal	240 (1st) and 90 (100th)	0.01–3.0	0.1 A g <sup>-1</sup>	436	2.65	81.6 (80th)	111
	cathode/SIB	one-step solvothermal	684.6 (1st)	0.01–3.0	10 A g <sup>-1</sup>	14.5	n/a	n/a	111
Cu <sub>9</sub> S <sub>4</sub> -AHP microspheres CuS nanoplates	anode/SIB	one-step solvothermal	312.5 (1000th)	0.3–3.2	100 mA g <sup>-1</sup>	n/a	1.5	94.3	112
	anode/SIB	solvothermal	429 (1st) and 386 (200th)	0.05–2.6	0.2 C	n/a	n/a	~100 (50th)	113
CuS microflower	anode/SIB	facile dealloying	680 (1st) and 560 (50th)	1.39–2.18	0.1 A g <sup>-1</sup>	67.9	1.0	90.9	114
	cathode/SIB	hydrothermal	483 (1st)	1.39–2.18	5 A g <sup>-1</sup>	n/a	n/a	n/a	115
3D flower-like CuS composite copper sulfide microspheres	cathode/SIB	hydrothermal	132.6 (5000th)	1.0–3.0	31 mA g <sup>-1</sup>	n/a	1.0	100 (several cycles)	116
	cathode/LIB	hydrothermal	348.6 (1st) and 41.8 (100th)	1.0–3.0	50 mA g <sup>-1</sup>	7.876	1.61–1.86	95.8 (200th)	117
Cu <sub>2</sub> S spheres	anode/SIB	microwave synthesis	169 (1st) and 162 (200th)	0.6–3.0	0.1 C	n/a	1.5–2.0	~100 (3rd)	118
	cathode/LIB	spray pyrolysis	328 (1st)	1.0–3.0	1 C	n/a	n/a	n/a	118
CuS spheres	cathode/LIB	spray pyrolysis	250 (100th)	1.0–3.0	0.02 C	n/a	1.5	100 (20th)	118
	cathode/LIB	spray pyrolysis	560 (1st)	1.2–3.0	0.02 C	n/a	1.5	100 (20th)	118
CuS@Sisal fiber carbon composite Cu <sub>9</sub> S <sub>4</sub> /NSC composite	anode/LIB	hydrothermal	440 (200th)	1.2–3.0	1 C	n/a	n/a	n/a	120
	anode/SIB	thermal treatment	903 (1st) and 303 (30th)	0.01–3.0	50 mA g <sup>-1</sup>	n/a	n/a	60.7	121
Cu <sub>2</sub> S nanoribbon CuS:	cathode/LIB	direct sulfurization	412 (1st) and 344.3 (200th)	0.01–3.0	100 mA g <sup>-1</sup>	65.5	1.3	n/a	121
	cathode/LIB	direct sulfurization	800 (1st)	1.00–3.0	50 mA g <sup>-1</sup>	n/a	n/a	n/a	63
hollow CuS nanocubes hollow CuS nanoboxes	cathode/LIB	hard template	170 (100th)	1.00–3.0	2500 mA g <sup>-1</sup>	n/a	n/a	n/a	39
	cathode/LIB	hard template	370 (1st)	1.00–3.0	50 mA g <sup>-1</sup>	n/a	n/a	n/a	39
hollow CuS nanoboxes	cathode/LIB	hard template	90 (100th)	0.01–2.5	2500 mA g <sup>-1</sup>	198.474	1.5	~100	39
	cathode/LIB	hard template	200 (1st)	0.01–2.5	100 mA g <sup>-1</sup>	n/a	1.5	~100	39
hollow CuS nanoboxes	cathode/LIB	hard template	50 (200th)	0.01–2.5	1000 mA g <sup>-1</sup>	n/a	1.5	99.8 (1300th)	124
	cathode/LIB	hard template	405 (1300th)	1.2–3.0	2 C	n/a	1.5–2.0	99.8 (1300th)	124



Table 1. continued

material	electrode/battery	synthesis method	electrochemical performance					ref	
			capacity, mAh g <sup>-1</sup> (cycle)	potential range, V	current rate	surface area, m <sup>2</sup> g <sup>-1</sup>	mass loading, mg cm <sup>-2</sup>		CE at first cycle, %
Cu <sub>1.8</sub> S with a hollow octahedral structure	anode/SIB	calcination, phase transition	403 (1st) and 250 (1000th)	0.5–2.2	2 C	n/a	n/a	~100 (1000th)	125
CuS@CoS <sub>2</sub> hollow nanoboxes	anode/SIB	hard template	625 (1st) and 79% initial capacity (500th)	0.4–2.52	0.5 A g <sup>-1</sup>	n/a	n/a	n/a	126
CuS hollow spheres	cathode/LIB	bubble template	480 (1st)	0.05–3	50 mA g <sup>-1</sup>	n/a	n/a	n/a	53
CuS hollow spheres and flower-like spheres	cathode/LIB	hydrothermal	401 (1st) and 75 (40th)	1.5–2.6	5 mA g <sup>-1</sup>	n/a	n/a	n/a	54
hollow pine-needle-like CuS	anode/SIB	reflux-assisted cosolvent	522 (1st)	0.3–3.0	0.1 A g <sup>-1</sup>	17.8 8	1.2–1.4	95	37
			436 (1000th)	0.3–3.0	5 A g <sup>-1</sup>				
CuS dandelion-like clusters	anode/LIB	colloidal	420 (1st) and 390 (10th)	1.0–3.0	0.56 A g <sup>-1</sup>	14.8	n/a	n/a	127
carbon-coated Cu <sub>9</sub> S <sub>5</sub> bullet-like hollow particles	anode/SIB	anion exchange–carbonization–cation exchange	385 (1st) and 79% retention (4000th)	0.4–2.6	0.3 A g <sup>-1</sup>	n/a	n/a	94	128
Cu <sub>2-x</sub> S@M (M = C, TiO <sub>2</sub> , MoS <sub>2</sub> ) hollow spheres	cathode/LIB	thermolysis synthesis	353 (1st)	1.0–3.0	400 mA g <sup>-1</sup>	14.4 (M = 1.6C)	1.2–1.8	~100 (200th)	99
			278 (1000th)	1.0–3.0	800 mA g <sup>-1</sup>				
CuS on Cu foam	cathode/LIB	electrochemical corrosion	570 (1st) and 845 (500th)	0.3–2.2	0.5 A g <sup>-1</sup>	n/a	n/a	n/a	129
Cu <sub>2</sub> S on the Cu foam	cathode/LIB	dry thermal sulfuration	0.74 (1st) and 0.41 mAh cm <sup>-2</sup> (100th)	0.02–3.0	0.25 C	n/a	38	97.8 (140th)	130
Cu <sub>x</sub> S on Cu foam									
Cu <sub>1.8</sub> S:	cathode/LIB	solution	240 (1st) and 250 (20th)	1.0–3.0	1.4 mAh	n/a	8.7–10.4	100 (20th)	131
Cu <sub>1.96</sub> S:			100 (1st) and 98 (20th)	1.0–3.0	1.4 mAh			100 (20th)	
		Full-Cells with Cu <sub>x</sub> S Electrodes							
N-doped CuS nanowires	anode/SIB	mixed solvent hydrothermal	406 (1st) and 220 (200th)	0.25–3.0	0.2 A g <sup>-1</sup>	30.6	1.8–2.1	99.3 (2nd)	132
CuS//NVPF/NVP (Fe 8.9%)	anode/SIB	commercial CuS	101 (1st)	0–4.25	1 C	n/a	n/a	95 (450th)	133
			90 (450th)	0–4.05	3 C				
CuS nanospheres	cathode/MIB	solvothermal method	138 (1st) and 80 (15th)	0.2–1.9	20 mA g <sup>-1</sup>	n/a	5–7	68.6	134

design of the structure of  $\text{Cu}_x\text{S}$  material depending on its simplicity/complexity and resources availability.

## ■ CONCLUSIONS

This review summarizes various design and synthesis approaches of diversified  $\text{Cu}_x\text{S}$  micro-/nanostructures that have been extensively developed and studied for application in the field of energy storage. The favorable effects of rational nanostructure engineering on the storage properties and performances of different rechargeable batteries have been discussed. To clearly understand the role of nanoengineering in obtaining the most performing  $\text{Cu}_x\text{S}$  this work has summarized the nanostructures based on their dimensionality starting from 0D to 3D. In general, all 0D–3D nanostructures have the advantages of improved electrochemical activity, shortened electronic/ionic diffusion path, enhanced electrical conductivity, and the capability to buffer volume change during conversion reaction in  $\text{Cu}_x\text{S}$ , all of which result in a high reversible capacity, enhanced rate capability, and long-term cyclability. The stated features are mainly derived from the small grain size, unique architecture, desired composition, and the existence of porous/hollow structures. Undoubtedly, wisely designed 0D–3D materials have a large surface area, high electron conductivity, and controllable structure. However, these materials require additional auxiliary components to function, which lead to a high percentage of passive components, decreasing the amount of energy density. In this regard, self-standing 3D electrodes can resolve this challenge, but the construction of a tricontinuous battery with active electrodes, a separator, and current collector is the main challenge.

According to the variations in dimensions, electrode materials indicate distinct electrochemical performance and cycling stability. Zero-dimensional nanoparticles of all active materials used in rechargeable batteries are believed to be the most favorable due to their simple and scalable production possibilities. However, in the case of  $\text{Cu}_x\text{S}$  nanoparticles, despite the improved performance resulting from the short ionic paths, the volume expansion and polysulfide dissolution still cannot be avoided. Furthermore, the complexity of synthesis is yet to be solved. The reported cycle life of half-cells of different rechargeable batteries constructed with  $\text{Cu}_x\text{S}$  nanoparticles did not even exceed 350 cycles, meaning that the nanoparticles have a long way to go to be applied practically.

One- and two-dimensional  $\text{Cu}_x\text{S}$  materials have been reported to show a better capability to withstand the volume change compared to nanoparticles and provide better electronic transportation and high surface area. Moreover, the combination of 1D–2D  $\text{Cu}_x\text{S}$  materials with rGO, graphene or carbon additives is an efficient strategy to trap the polysulfides and diminish the volume change. Nonetheless, despite many efforts, capacity retention of these structures still leaves a lot to be desired.

From the viewpoint of 3D structures, the cavity of intricate hollow structures can effectively accommodate the volume change of  $\text{Cu}_x\text{S}$  and can help to avoid the discharged products from dissolution through either physical confinement or chemical interactions. Thin nanowalls provide fast diffusion and large areas of the outer and inner surfaces contribute to better electrolyte infiltration exposing more active sites for reaction. The outstanding performance of up to 5000 cycles was achieved. However, the cumbersome synthesis process and

reduced tapping density have to be optimized before being considered for practical applications.

Recent high interest in the self-standing 3D structures for  $\text{Cu}_x\text{S}$  showed a great potential of such materials in LIB, NIB, AIB, and MIB. However, the performance of such structures comes at a price of compromised volumetric energy density of the electrodes to some extent. The difficulties of synthesizing such complex morphologies need more optimization and attention for the all-in-one structure batteries. For instance, a new type of 3D batteries consisting of layers of cathode, anode, and electrolyte within one structure is attracting more attention in the current days.

Even though considerable advances have been achieved in designing and exploring the various kinds of  $\text{Cu}_x\text{S}$  nanostructures and their application in rechargeable batteries, many challenges still remain as it is extremely hard to design  $\text{Cu}_x\text{S}$  nanostructured materials that would offer high rate capability, large capacity, and long cycle life at the same time.

Regardless of the awaiting challenges ahead with the new technologies' rapid development and growing enthusiasm from researchers around the world, more advanced nanostructured  $\text{Cu}_x\text{S}$  electrodes with outstanding performance will be developed and studied for energy storage. No doubt that one day we might be using a device powered by the rechargeable battery based on  $\text{Cu}_x\text{S}$  material. More investigations for inexpensive and straightforward synthesis methods with the unique morphological structures will lead this field to the spot of the next-generation battery not only for portable devices but also to the full-scale development of EVs.

## ■ AUTHOR INFORMATION

### Corresponding Author

Zhumabay Bakenov – National Laboratory Astana and Department of Chemical and Materials Engineering, Nazarbayev University, Nur-Sultan 010000, Kazakhstan; [orcid.org/0000-0003-2781-4955](https://orcid.org/0000-0003-2781-4955); Email: [zbakenov@nu.edu.kz](mailto:zbakenov@nu.edu.kz)

### Authors

Gulnur Kalimuldina – Department of Mechanical and Aerospace Engineering, Nazarbayev University, Nur-Sultan 010000, Kazakhstan; [orcid.org/0000-0001-9185-3217](https://orcid.org/0000-0001-9185-3217)

Arailym Nurpeissova – National Laboratory Astana, Nazarbayev University, Nur-Sultan 010000, Kazakhstan

Assyl Adylkhanova – Department of Chemical and Materials Engineering, Nazarbayev University, Nur-Sultan 010000, Kazakhstan

Desmond Adair – Department of Mechanical and Aerospace Engineering, Nazarbayev University, Nur-Sultan 010000, Kazakhstan

Izumi Taniguchi – Department of Chemical Science and Engineering, Tokyo Institute of Technology, Tokyo 152-8552, Japan

Complete contact information is available at: <https://pubs.acs.org/10.1021/acsaem.0c01686>

### Notes

The authors declare no competing financial interest.

## ■ ACKNOWLEDGMENTS

This work was supported by the research grants 091019CRP2114 “Three-Dimensional All Solid State Rechargeable Batteries” and 240919FD3914 “Self-Charging



Rechargeable Lithium-ion Battery” from Nazarbayev University and the research projects AP05133706 “Innovative High-Capacity Anodes Based on Lithium Titanate for a Next Generation of Batteries” and AP08052143 “Development of Wearable Self-Charging Power Unit” from the Ministry of Education and Science of the Republic of Kazakhstan.

## REFERENCES

- (1) Wang, Y.; Zhang, X.; Chen, P.; Liao, H.; Cheng, S. In Situ Preparation of CuS Cathode with Unique Stability and High Rate Performance for Lithium Ion Batteries. *Electrochim. Acta* **2012**, *80*, 264–268.
- (2) Nazir, H.; Batool, M.; Bolivar Osorio, F. J.; Isaza-Ruiz, M.; Xu, X.; Vignarooban, K.; Phelan, P.; Inamuddin; Kannan, A. M. Recent Developments in Phase Change Materials for Energy Storage Applications: A Review. *Int. J. Heat Mass Transfer* **2019**, *129*, 491–523.
- (3) Koochi-Fayegh, S.; Rosen, M. A. A Review of Energy Storage Types, Applications and Recent Developments. *J. Energy Storage* **2020**, *27*, 101047.
- (4) Ye, J.; Baumgaertel, A. C.; Wang, Y. M.; Biener, J.; Biener, M. M. Structural Optimization of 3D Porous Electrodes for High-Rate Performance Lithium Ion Batteries. *ACS Nano* **2015**, *9* (2), 2194–2202.
- (5) Kisu, K.; Aoyagi, S.; Nagatomo, H.; Iwama, E.; Reid, M. T. H.; Naoi, W.; Naoi, K. Internal Resistance Mapping Preparation to Optimize Electrode Thickness and Density Using Symmetric Cell for High-Performance Lithium-Ion Batteries and Capacitors. *J. Power Sources* **2018**, *396* (April), 207–212.
- (6) Kasnatscheew, J.; Wagner, R.; Winter, M.; Cekic-Laskovic, I. Interfaces and Materials in Lithium Ion Batteries: Challenges for Theoretical Electrochemistry. *Top. Curr. Chem.* **2018**, *376* (3), 1–29.
- (7) Mei, W.; Chen, H.; Sun, J.; Wang, Q. The Effect of Electrode Design Parameters on Battery Performance and Optimization of Electrode Thickness Based on the Electrochemical-Thermal Coupling Model. *Sustain. Energy Fuels* **2019**, *3* (1), 148–165.
- (8) Lu, C. H.; Lin, S. W. Influence of the Particle Size on the Electrochemical Properties of Lithium Manganese Oxide. *J. Power Sources* **2001**, *97–98*, 458–460.
- (9) Fergus, J. W. Recent Developments in Cathode Materials for Lithium Ion Batteries. *J. Power Sources* **2010**, *195* (4), 939–954.
- (10) Zhao, R.; Liu, J.; Gu, J. The Effects of Electrode Thickness on the Electrochemical and Thermal Characteristics of Lithium Ion Battery. *Appl. Energy* **2015**, *139*, 220–229.
- (11) Newman, J. Optimization of Porosity and Thickness of a Battery Electrode by Means of a Reaction-Zone Model. *J. Electrochem. Soc.* **1995**, *142* (1), 97.
- (12) Xiao, L.; Guo, Y.; Qu, D.; Deng, B.; Liu, H.; Tang, D. Influence of Particle Sizes and Morphologies on the Electrochemical Performances of Spinel LiMn<sub>2</sub>O<sub>4</sub> Cathode Materials. *J. Power Sources* **2013**, *225*, 286–292.
- (13) Zheng, H.; Li, J.; Song, X.; Liu, G.; Battaglia, V. S. A Comprehensive Understanding of Electrode Thickness Effects on the Electrochemical Performances of Li-Ion Battery Cathodes. *Electrochim. Acta* **2012**, *71*, 258–265.
- (14) Kasnatscheew, J.; Rodehorst, U.; Streipert, B.; Wiemers-Meyer, S.; Jakelski, R.; Wagner, R.; Laskovic, I. C.; Winter, M. Learning from Overpotentials in Lithium Ion Batteries: A Case Study on the LiNi<sub>1/3</sub>Co<sub>1/3</sub>Mn<sub>1/3</sub>O<sub>2</sub> (NCM) Cathode. *J. Electrochem. Soc.* **2016**, *163* (14), A2943–A2950.
- (15) Li, J.; Cameron, A. R.; Li, H.; Glazier, S.; Xiong, D.; Chatzidakis, M.; Allen, J.; Botton, G. A.; Dahn, J. R. Comparison of Single Crystal and Polycrystalline LiNi<sub>0.5</sub>Mn<sub>0.3</sub>Co<sub>0.2</sub>O<sub>2</sub> Positive Electrode Materials for High Voltage Li-Ion Cells. *J. Electrochem. Soc.* **2017**, *164* (7), A1534–A1544.
- (16) Qu, D. Fundamental Principles of Battery Design: Porous Electrodes. *AIP Conf. Proc.* **2013**, *1597*, 14–25.
- (17) Kalluri, S.; Yoon, M.; Jo, M.; Park, S.; Myeong, S.; Kim, J.; Dou, S. X.; Guo, Z.; Cho, J. Surface Engineering Strategies of Layered LiCoO<sub>2</sub> Cathode Material to Realize High-Energy and High-Voltage Li-Ion Cells. *Adv. Energy Mater.* **2017**, *7* (1), 1601507.
- (18) Mendoza, H.; Roberts, S. A.; Brunini, V. E.; Grillet, A. M. Mechanical and Electrochemical Response of a LiCoO<sub>2</sub> Cathode Using Reconstructed Microstructures. *Electrochim. Acta* **2016**, *190*, 1–15.
- (19) De Las Casas, C.; Li, W. A Review of Application of Carbon Nanotubes for Lithium Ion Battery Anode Material. *J. Power Sources* **2012**, *208*, 74–85.
- (20) Palacín, M. R. Recent Advances in Rechargeable Battery Materials: A Chemist’s Perspective. *Chem. Soc. Rev.* **2009**, *38* (9), 2565–2575.
- (21) Goriparti, S.; Miele, E.; De Angelis, F.; Di Fabrizio, E.; Proietti Zaccaria, R.; Capiglia, C. Review on Recent Progress of Nanostructured Anode Materials for Li-Ion Batteries. *J. Power Sources* **2014**, *257*, 421–443.
- (22) Pan, Q.; Xie, J.; Liu, S.; Cao, G.; Zhu, T.; Zhao, X. Facile One-Pot Synthesis of Ultrathin NiS Nanosheets Anchored on Graphene and the Improved Electrochemical Li-Storage Properties. *RSC Adv.* **2013**, *3* (12), 3899–3906.
- (23) Liu, J.; Wu, C.; Xiao, D.; Kopold, P.; Gu, L.; Van Aken, P. A.; Maier, J.; Yu, Y. MOF-Derived Hollow Co<sub>9</sub>S<sub>8</sub> Nanoparticles Embedded in Graphitic Carbon Nanocages with Superior Li-Ion Storage. *Small* **2016**, *12* (17), 2354–2364.
- (24) Lu, M.; Liao, C.; Jiang, C.; Du, Y.; Zhang, Z.; Wu, S. Remarkable High-Temperature Performance of Hollow Co<sub>9</sub>S<sub>8</sub> Nanoparticles Integrated with Carbon Materials for Lithium-Ion Batteries. *Electrochim. Acta* **2017**, *250*, 196–202.
- (25) He, J.; Li, Q.; Chen, Y.; Xu, C.; Zhou, K.; Wang, X.; Zhang, W.; Li, Y. Self-Assembled Cauliflower-like FeS<sub>2</sub> Anchored into Graphene Foam as Free-Standing Anode for High-Performance Lithium-Ion Batteries. *Carbon* **2017**, *114*, 111–116.
- (26) Jache, B.; Mogwitz, B.; Klein, F.; Adelhelm, P. Copper Sulfides for Rechargeable Lithium Batteries: Linking Cycling Stability to Electrolyte Composition. *J. Power Sources* **2014**, *247*, 703–711.
- (27) Jiang, K.; Chen, Z.; Meng, X. CuS and Cu<sub>2</sub>S as Cathode Materials for Lithium Batteries: A Review. *ChemElectroChem* **2019**, *6*, 2825–2840.
- (28) Xu, X.; Liu, W.; Kim, Y.; Cho, J. Nanostructured Transition Metal Sulfides for Lithium Ion Batteries: Progress and Challenges. *Nano Today* **2014**, *9* (5), 604–630.
- (29) Bhattacharjya, D.; Sinhamahapatra, A.; Ko, J. J.; Yu, J. S. High Capacity and Exceptional Cycling Stability of Ternary Metal Sulfide Nanorods as Li Ion Battery Anodes. *Chem. Commun.* **2015**, *51* (69), 13350–13353.
- (30) Fei, L.; Williams, B. P.; Yoo, S. H.; Carlin, J. M.; Joo, Y. L. A General Approach to Fabricate Free-Standing Metal Sulfide@carbon Nanofiber Networks as Lithium Ion Battery Anodes. *Chem. Commun.* **2016**, *52* (7), 1501–1504.
- (31) Rui, X.; Tan, H.; Yan, Q. Nanostructured Metal Sulfides for Energy Storage. *Nanoscale* **2014**, *6* (17), 9889–9924.
- (32) Lai, C. H.; Lu, M. Y.; Chen, L. J. Metal Sulfide Nanostructures: Synthesis, Properties and Applications in Energy Conversion and Storage. *J. Mater. Chem.* **2012**, *22* (1), 19–30.
- (33) Débart, A.; Dupont, L.; Patrice, R.; Tarascon, J. M. Reactivity of Transition Metal (Co, Ni, Cu) Sulphides versus Lithium: The Intriguing Case of the Copper Sulphide. *Solid State Sci.* **2006**, *8* (6), 640–651.
- (34) Kalimuldina, G.; Taniguchi, I. Synthesis and Electrochemical Characterization of Stoichiometric Cu<sub>2</sub>S as Cathode Material with High Rate Capability for Rechargeable Lithium Batteries. *J. Power Sources* **2016**, *331*, 258–266.
- (35) Chung, J. S.; Sohn, H. J. Electrochemical Behaviors of CuS as a Cathode Material for Lithium Secondary Batteries. *J. Power Sources* **2002**, *108* (1–2), 226–231.

- (36) Wu, H.; Li, T.; Li, H.; Zhang, D.; Xu, F. Sodium-Storage Performance of CuS Microspheres with Hydroxyl Hyperbranched Polyamide Additive. *Mater. Lett.* **2020**, *262*, 127181.
- (37) Yu, D.; Li, M.; Yu, T.; Wang, C.; Zeng, Y.; Hu, X.; Chen, G.; Yang, G.; Du, F. Nanotube-Assembled Pine-Needle-like CuS as an Effective Energy Booster for Sodium-Ion Storage. *J. Mater. Chem. A* **2019**, *7* (17), 10619–10628.
- (38) Wang, S.; Jiao, S.; Wang, J.; Chen, H.-S.; Tian, D.; Lei, H.; Fang, D.-N. High-Performance Aluminum-Ion Battery with CuS@C Microsphere Composite Cathode. *ACS Nano* **2017**, *11* (1), 469–477.
- (39) Shen, J.; Zhang, Y.; Chen, D.; Li, X.; Chen, Z.; Cao, S. A.; Li, T.; Xu, F. A Hollow CuS Nanocube Cathode for Rechargeable Mg Batteries: Effect of the Structure on the Performance. *J. Mater. Chem. A* **2019**, *7* (37), 21410–21420.
- (40) MacHani, T.; Rossi, D. P.; Golden, B. J.; Jones, E. C.; Lotfipour, M.; Plass, K. E. Synthesis of Monoclinic and Tetragonal Chalcocite Nanoparticles by Iron-Induced Stabilization. *Chem. Mater.* **2011**, *23* (24), 5491–5495.
- (41) Okamoto, K.; Kawai, S. Electrical Conduction and Phase Transition of Copper Sulfides. *Jpn. J. Appl. Phys.* **1973**, *12* (8), 1130–1138.
- (42) Chaki, S. H.; Tailor, J. P.; Deshpande, M. P. Covellite CuS - Single Crystal Growth by Chemical Vapour Transport (CVT) Technique and Characterization. *Mater. Sci. Semicond. Process.* **2014**, *27* (1), 577–585.
- (43) Jeevanandam, J.; Barhoum, A.; Chan, Y. S.; Dufresne, A.; Danquah, M. K. Review on Nanoparticles and Nanostructured Materials: History, Sources, Toxicity and Regulations. *Beilstein J. Nanotechnol.* **2018**, *9* (1), 1050–1074.
- (44) Pokropivny, V. V.; Skorokhod, V. V. Classification of Nanostructures by Dimensionality and Concept of Surface Forms Engineering in Nanomaterial Science. *Mater. Sci. Eng., C* **2007**, *27* (5–8), 990–993.
- (45) Li, X.; He, X.; Shi, C.; Liu, B.; Zhang, Y.; Wu, S.; Zhu, Z.; Zhao, J. Synthesis of One-Dimensional Copper Sulfide Nanorods as High-Performance Anode in Lithium Ion Batteries. *ChemSusChem* **2014**, *7* (12), 3328–3333.
- (46) Tiwari, J. N.; Tiwari, R. N.; Kim, K. S. Zero-Dimensional, One-Dimensional, Two-Dimensional and Three-Dimensional Nanostructured Materials for Advanced Electrochemical Energy Devices. *Prog. Mater. Sci.* **2012**, *57* (4), 724–803.
- (47) Dhasade, S. S.; Patil, J. S.; Kim, J. H.; Han, S. H.; Rath, M. C.; Fulari, V. J. Synthesis of CuS Nanorods Grown at Room Temperature by Electrodeposition Method. *Mater. Chem. Phys.* **2012**, *137* (1), 353–358.
- (48) Wang, Z.; Zhang, X.; Zhang, Y.; Li, M.; Qin, C.; Bakenov, Z. Chemical Dealloying Synthesis of CuS Nanowire-on-Nanoplate Network as Anode Materials for Li-Ion Batteries. *Metals (Basel, Switz.)* **2018**, *8* (4), 252.
- (49) Feng, C.; Zhang, L.; Yang, M.; Song, X.; Zhao, H.; Jia, Z.; Sun, K.; Liu, G. One-Pot Synthesis of Copper Sulfide Nanowires/Reduced Graphene Oxide Nanocomposites with Excellent Lithium-Storage Properties as Anode Materials for Lithium-Ion Batteries. *ACS Appl. Mater. Interfaces* **2015**, *7* (29), 15726–15734.
- (50) Ren, Y.; Wei, H.; Yang, B.; Wang, J.; Ding, J. Double-Sandwich-Like CuS@reduced Graphene Oxide as an Anode in Lithium Ion Batteries with Enhanced Electrochemical Performance. *Electrochim. Acta* **2014**, *145*, 193–200.
- (51) Phuruangrat, A.; Thongtem, S.; Thongtem, T. Microwave Hydrothermal Synthesis and Characterization of Copper Sulfide with Different Morphologies. *Chalcogenide Lett.* **2013**, *10* (10), 359–365.
- (52) Ni, S.; Li, T.; Yang, X. Fabrication of Cu<sub>2</sub>S on Cu Film Electrode and Its Application in Lithium Ion Battery. *Thin Solid Films* **2012**, *520* (21), 6705–6708.
- (53) Zhao, L.; Tao, F.; Quan, Z.; Zhou, X.; Yuan, Y.; Hu, J. Bubble Template Synthesis of Copper Sulfide Hollow Spheres and Their Applications in Lithium Ion Battery. *Mater. Lett.* **2012**, *68*, 28–31.
- (54) Nagarathinam, M.; Saravanan, K.; Leong, W. L.; Balaya, P.; Vittal, J. J. Hollow Nanospheres and Flowers of CuS from Self-Assembled Cu(II) Coordination Polymer and Hydrogen-Bonded Complexes of N-(2-Hydroxybenzyl)-L-Serine. *Cryst. Growth Des.* **2009**, *9* (10), 4461–4470.
- (55) Xu, M.; Wu, H.; Da, P.; Zhao, D.; Zheng, G. Unconventional 0-, 1-, and 2-Dimensional Single-Crystalline Copper Sulfide Nanostructures. *Nanoscale* **2012**, *4* (5), 1794.
- (56) Wu, M.; Zhang, Y.; Li, T.; Chen, Z.; Cao, S. A.; Xu, F. Copper Sulfide Nanoparticles as High-Performance Cathode Materials for Magnesium Secondary Batteries. *Nanoscale* **2018**, *10* (26), 12526–12534.
- (57) Kravchik, K. V.; Widmer, R.; Erni, R.; Dubey, R. J. C.; Krumeich, F.; Kovalenko, M. V.; Bodnarchuk, M. I. Copper Sulfide Nanoparticles as High-Performance Cathode Materials for Mg-Ion Batteries. *Sci. Rep.* **2019**, *9* (1), 1–8.
- (58) Liu, Y.; Jin, B.; Zhu, Y. F.; Ma, X. Z.; Lang, X. Y. Synthesis of Cu<sub>2</sub>S/Carbon Composites with Improved Lithium Storage Performance. *Int. J. Hydrogen Energy* **2015**, *40* (1), 670–674.
- (59) Pan, J.; Shen, H.; Mathur, S. One-Dimensional SnO<sub>2</sub> Nanostructures: Synthesis and Applications. *J. Nanotechnol.* **2012**, *20*, 1.
- (60) Ge, M.; Cao, C.; Huang, J.; Li, S.; Chen, Z.; Zhang, K. Q.; Al-Deyab, S. S.; Lai, Y. A Review of One-Dimensional TiO<sub>2</sub> Nanostructured Materials for Environmental and Energy Applications. *J. Mater. Chem. A* **2016**, *4* (18), 6772–6801.
- (61) Mu, C.; He, J. Synthesis of Single Crystal Metal Sulfide Nanowires and Nanowire Arrays by Chemical Precipitation in Templates. *J. Nanosci. Nanotechnol.* **2010**, *10* (12), 8191–8198.
- (62) Wu, C.; Shi, J.-B.; Chen, C.-J.; Chen, Y.-C.; Lin, Y.-T.; Wu, P.-F.; Wei, S.-Y. Synthesis and Optical Properties of CuS Nanowires Fabricated by Electrodeposition with Anodic Alumina Membrane. *Mater. Lett.* **2008**, *62* (6–7), 1074–1077.
- (63) Wen, X.; Zhang, W.; Yang, S.; Dai, Z. R.; Wang, Z. L. Solution Phase Synthesis of Cu(OH)<sub>2</sub> Nanoribbons by Coordination Self-Assembly Using Cu<sub>2</sub>S Nanowires as Precursors. *Nano Lett.* **2002**, *2* (12), 1397–1401.
- (64) Foley, S.; Geaney, H.; Bree, G.; Stokes, K.; Connolly, S.; Zaworotko, M. J.; Ryan, K. M. Copper Sulfide (Cu<sub>2</sub>S) Nanowire-in-Carbon Composites Formed from Direct Sulfurization of the Metal-Organic Framework HKUST-1 and Their Use as Li-Ion Battery Cathodes. *Adv. Funct. Mater.* **2018**, *28* (19), 1800587.
- (65) Ghahremaninezhad, A.; Asselin, E.; Dixon, D. G. One-Step Template-Free Electrosynthesis of 300 Mm Long Copper Sulfide Nanowires. *Electrochem. Commun.* **2011**, *13* (1), 12–15.
- (66) Chen, Y. C.; Shi, J. B.; Wu, C.; Chen, C. J.; Lin, Y. T.; Wu, P. F. Fabrication and Optical Properties of CuS Nanowires by Sulfuring Method. *Mater. Lett.* **2008**, *62* (8–9), 1421–1423.
- (67) Chen, L. J. Silicon Nanowires: The Key Building Block for Future Electronic Devices. *J. Mater. Chem.* **2007**, *17* (44), 4639–4643.
- (68) Law, M.; Greene, L. E.; Johnson, J. C.; Saykally, R.; Yang, P. Nanowire Dye-Sensitized Solar Cells. *Nat. Mater.* **2005**, *4* (6), 455–459.
- (69) Cui, L.-F.; Yang, Y.; Hsu, C.-M.; Cui, Y. Carbon-Silicon Core-Shell Nanowires as High Capacity Electrode for Lithium Ion Batteries. *Nano Lett.* **2009**, *9* (9), 3370–3374.
- (70) Tian, M.; Wang, W.; Wei, Y.; Yang, R. Stable High Areal Capacity Lithium-Ion Battery Anodes Based on Three-Dimensional Ni-Sn Nanowire Networks. *J. Power Sources* **2012**, *211*, 46–51.
- (71) Taylor, R. L. American Association for the Advancement of Science. *J. Clin. Endocrinol. Metab.* **1950**, *10* (10), 1361–1362.
- (72) Lai, C.-H.; Huang, K.-W.; Cheng, J.-H.; Lee, C.-Y.; Lee, W.-F.; Huang, C.-T.; Hwang, B.-J.; Chen, L.-J. Oriented Growth of Large-Scale Nickel Sulfide Nanowire Arrays via a General Solution Route for Lithium-Ion Battery Cathode Applications. *J. Mater. Chem.* **2009**, *19* (39), 7277–7283.
- (73) Lai, C. H.; Huang, K. W.; Cheng, J. H.; Lee, C. Y.; Hwang, B. J.; Chen, L. J. Direct Growth of High-Rate Capability and High Capacity Copper Sulfide Nanowire Array Cathodes for Lithium-Ion Batteries. *J. Mater. Chem.* **2010**, *20* (32), 6638–6645.



- (74) Meng, X.; Riha, S. C.; Libera, J. A.; Wu, Q.; Wang, H. H.; Martinson, A. B. F.; Elam, J. W. Tunable Core-Shell Single-Walled Carbon Nanotube-Cu<sub>2</sub>S Networked Nanocomposites as High-Performance Cathodes for Lithium-Ion Batteries. *J. Power Sources* **2015**, *280*, 621–629.
- (75) Zhou, M.; Peng, N.; Liu, Z.; Xi, Y.; He, H.; Xia, Y.; Liu, Z.; Okada, S. Synthesis of Sub-10 Nm Copper Sulphide Rods as High-Performance Anode for Long-Cycle Life Li-Ion Batteries. *J. Power Sources* **2016**, *306*, 408–412.
- (76) Cai, R.; Chen, J.; Zhu, J.; Xu, C.; Zhang, W.; Zhang, C.; Shi, W.; Tan, H.; Yang, D.; Hng, H. H.; Lim, T. M.; Yan, Q. Synthesis of Cu x S/Cu Nanotubes and Their Lithium Storage Properties. *J. Phys. Chem. C* **2012**, *116* (23), 12468–12474.
- (77) Han, F.; Li, W. C.; Li, D.; Lu, A. H. In Situ Electrochemical Generation of Mesoporous Cu<sub>2</sub>S/C Composite for Enhanced Lithium Storage: Mechanism and Material Properties. *ChemElectroChem* **2014**, *1* (4), 733–740.
- (78) Yang, S.; Ran, Y.; Wu, H.; Wang, S.; Feng, C.; Li, G. Hydrothermal Synthesis of Copper Sulfide Flowers and Nanorods for Lithium-Ion Battery Applications. *Nanosci. Nanotechnol. Res.* **2018**, *2*, 7.
- (79) Chen, Q.; Ren, M.; Xu, H.; Liu, W.; Hei, J.; Su, L.; Wang, L. Cu<sub>2</sub>S@N, S Dual-Doped Carbon Matrix Hybrid as Superior Anode Materials for Lithium/Sodium Ion Batteries. *ChemElectroChem* **2018**, *5* (15), 2135–2141.
- (80) Schwierz, F.; Pezoldt, J.; Granzner, R. Two-Dimensional Materials and Their Prospects in Transistor Electronics. *Nanoscale* **2015**, *7* (18), 8261–8283.
- (81) Fiori, G.; Bonaccorso, F.; Iannaccone, G.; Palacios, T.; Neumaier, D.; Seabaugh, A.; Banerjee, S. K.; Colombo, L. Electronics Based on Two-Dimensional Materials. *Nat. Nanotechnol.* **2014**, *9* (10), 768–779.
- (82) Naguib, M.; Mochalin, V. N.; Barsoum, M. W.; Gogotsi, Y. 25th Anniversary Article: MXenes: A New Family of Two-Dimensional Materials. *Adv. Mater.* **2014**, *26* (7), 992–1005.
- (83) Chen, K. S.; Balla, I.; Luu, N. S.; Hersam, M. C. Emerging Opportunities for Two-Dimensional Materials in Lithium-Ion Batteries. *ACS Energy Lett.* **2017**, *2* (9), 2026–2034.
- (84) Peng, L.; Zhu, Y.; Chen, D.; Ruoff, R. S.; Yu, G. Two-Dimensional Materials for Beyond-Lithium-Ion Batteries. *Adv. Energy Mater.* **2016**, *6* (11), 1600025.
- (85) Bhimanapati, G. R.; Lin, Z.; Meunier, V.; Jung, Y.; Cha, J.; Das, S.; Xiao, D.; Son, Y.; Strano, M. S.; Cooper, V. R.; Liang, L.; Louie, S. G.; Ringe, E.; Zhou, W.; Kim, S. S.; Naik, R. R.; Sumpter, B. G.; Terrones, H.; Xia, F.; Wang, Y.; Zhu, J.; Akinwande, D.; Alem, N.; Schuller, J. A.; Schaak, R. E.; Terrones, M.; Robinson, J. A. Recent Advances in Two-Dimensional Materials beyond Graphene. *ACS Nano* **2015**, *9* (12), 11509–11539.
- (86) Wang, X.; Weng, Q.; Yang, Y.; Bando, Y.; Golberg, D. Hybrid Two-Dimensional Materials in Rechargeable Battery Applications and Their Microscopic Mechanisms. *Chem. Soc. Rev.* **2016**, *45* (15), 4042–4073.
- (87) Kalimuldina, G.; Taniguchi, I. Electrochemical Properties of Stoichiometric CuS Coated on Carbon Fiber Paper and Cu Foil Current Collectors as Cathode Material for Lithium Batteries. *J. Mater. Chem. A* **2017**, *5* (15), 6937–6946.
- (88) Wang, Y.; Zhang, Y.; Li, H.; Peng, Y.; Li, J.; Wang, J.; Hwang, B. J.; Zhao, J. Realizing High Reversible Capacity: 3D Intertwined CNTs Inherently Conductive Network for CuS as an Anode for Lithium Ion Batteries. *Chem. Eng. J.* **2018**, *332*, 49–56.
- (89) Liu, H.; Zhou, W.; Zhang, Y. One-Pot Solvothermal Synthesis of CuS-CNTs Hybrid as Binder-Free Anode Material for Lithium Ion Batteries. *Colloids Interface Sci. Commun.* **2016**, *15*, 1–4.
- (90) Tao, H. C.; Yang, X. L.; Zhang, L. L.; Ni, S. B. One-Pot Facile Synthesis of CuS/Graphene Composite as Anode Materials for Lithium Ion Batteries. *J. Phys. Chem. Solids* **2014**, *75* (11), 1205–1209.
- (91) Ding, C.; Su, D.; Ma, W.; Zhao, Y.; Yan, D.; Li, J.; Jin, H. Design of Hierarchical CuS/Graphene Architectures with Enhanced Lithium Storage Capability. *Appl. Surf. Sci.* **2017**, *403*, 1–8.
- (92) Iqbal, S.; Bahadur, A.; Saeed, A.; Zhou, K.; Shoaib, M.; Waqas, M. Electrochemical Performance of 2D Polyaniline Anchored CuS/Graphene Nano-Active Composite as Anode Material for Lithium-Ion Battery. *J. Colloid Interface Sci.* **2017**, *502*, 16–23.
- (93) Yuan, D.; Huang, G.; Zhang, F.; Yin, D.; Wang, L. Facile Synthesis of CuS/RGO Composite with Enhanced Electrochemical Lithium-Storage Properties through Microwave-Assisted Hydrothermal Method. *Electrochim. Acta* **2016**, *203*, 238–245.
- (94) Li, H.; Wang, Y.; Huang, J.; Zhang, Y.; Zhao, J. Microwave-Assisted Synthesis of CuS/Graphene Composite for Enhanced Lithium Storage Properties. *Electrochim. Acta* **2017**, *225*, 443–451.
- (95) Li, J.; Yan, D.; Lu, T.; Qin, W.; Yao, Y.; Pan, L. Significantly Improved Sodium-Ion Storage Performance of Cus Nanosheets Anchored into Reduced Graphene Oxide with Ether-Based Electrolyte. *ACS Appl. Mater. Interfaces* **2017**, *9* (3), 2309–2316.
- (96) Zhang, Y.; Li, K.; Wang, Y.; Zeng, J.; Ji, P.; Zhao, J. Copper Sulfide Microspheres Wrapped with Reduced Graphene Oxide for High-Capacity Lithium-Ion Storage. *Mater. Sci. Eng., B* **2016**, *213*, 57–62.
- (97) Wang, J.; Lyu, X.; Wang, L.; Yu, S.; Zhu, W.; Han, C.; Cao, X. Preparation and Electrochemical Performance of Hierarchical CuS-RGO Composite. *J. Alloys Compd.* **2017**, *694*, 1067–1072.
- (98) Fan, X.; Sun, W.; Meng, F.; Xing, A.; Liu, J. Advanced Chemical Strategies for Lithium-Sulfur Batteries: A Review. *Green Energy Environ.* **2018**, *3* (1), 2–19.
- (99) Wang, Y.; Li, H.; Zhang, Y.; Peng, Y.; Zhang, P.; Zhao, J. Self-Templating Thermolysis Synthesis of Cu<sub>2</sub>-XS@M (M = C, TiO<sub>2</sub>, MoS<sub>2</sub>) Hollow Spheres and Their Application in Rechargeable Lithium Batteries. *Nano Res.* **2018**, *11* (2), 831–844.
- (100) Zhang, Z.; An, Y.; Feng, J.; Ci, L.; Duan, B.; Huang, W.; Dong, C.; Xiong, S. Carbon Coated Copper Sulfides Nanosheets Synthesized via Directly Sulfurizing Metal-Organic Frameworks for Lithium Batteries. *Mater. Lett.* **2016**, *181*, 340–344.
- (101) Kim, N. R.; Choi, J.; Yoon, H. J.; Lee, M. E.; Son, S. U.; Jin, H. J.; Yun, Y. S. Conversion Reaction of Copper Sulfide Based Nanohybrids for Sodium-Ion Batteries. *ACS Sustainable Chem. Eng.* **2017**, *5* (11), 9802–9808.
- (102) Park, J. Y.; Kim, S. J.; Yim, K.; Dae, K. S.; Lee, Y.; Dao, K. P.; Park, J. S.; Jeong, H. B.; Chang, J. H.; Seo, H. K.; Ahn, C. W.; Yuk, J. M. Pulverization-Tolerance and Capacity Recovery of Copper Sulfide for High-Performance Sodium Storage. *Adv. Sci.* **2019**, *6* (12), 1900264.
- (103) Chen, Y.; Davoisne, C.; Tarascon, J. M.; Guéry, C. Growth of Single-Crystal Copper Sulfide Thin Films via Electrodeposition in Ionic Liquid Media for Lithium Ion Batteries. *J. Mater. Chem.* **2012**, *22* (12), 5295–5299.
- (104) Xiao, S.; Li, X.; Sun, W.; Guan, B.; Wang, Y. General and Facile Synthesis of Metal Sulfide Nanostructures: In Situ Microwave Synthesis and Application as Binder-Free Cathode for Li-Ion Batteries. *Chem. Eng. J.* **2016**, *306*, 251–259.
- (105) Mazor, H.; Golodnitsky, D.; Burstein, L.; Peled, E. High Power Copper Sulfide Cathodes for Thin-Film Microbatteries. *Electrochem. Solid-State Lett.* **2009**, *12* (12), A232–A235.
- (106) National Research Council. *Hierarchical Structures in Biology as a Guide for New Materials Technology*; The National Academies Press: Washington, DC, USA, 1994; DOI: 10.17226/2215.
- (107) Chen, G.-Y.; Wei, Z.-Y.; Jin, B.; Zhong, X.-B.; Wang, H.; Zhang, W.-X.; Liang, J.-C.; Jiang, Q. Hydrothermal Synthesis of Copper Sulfide with Novel Hierarchical Structures and Its Application in Lithium-Ion Batteries. *Appl. Surf. Sci.* **2013**, *277*, 268–271.
- (108) Zhang, B.; Gao, X. W.; Wang, J. Z.; Chou, S. L.; Konstantinov, K.; Liu, H. K. CuS Nanoflakes, Microspheres, Microflowers, and Nanowires: Synthesis and Lithium Storage Properties. *J. Nanosci. Nanotechnol.* **2013**, *13*, 1309–1316.
- (109) Han, Y.; Wang, Y.; Gao, W.; Wang, Y.; Jiao, L.; Yuan, H.; Liu, S. Synthesis of Novel CuS with Hierarchical Structures and Its



Application in Lithium-Ion Batteries. *Powder Technol.* **2011**, *212* (1), 64–68.

(110) Sun, L.; Li, H.; Zhao, M.; Wang, G. High-Performance Lithium-Sulfur Batteries Based on Self-Supporting Graphene/Carbon Nanotube Foam@sulfur Composite Cathode and Quasi-Solid-State Polymer Electrolyte. *Chem. Eng. J.* **2018**, *332*, 8–15.

(111) Xiao, Y.; Su, D.; Wang, X.; Wu, S.; Zhou, L.; Shi, Y.; Fang, S.; Cheng, H. M.; Li, F. CuS Microspheres with Tunable Interlayer Space and Micropore as a High-Rate and Long-Life Anode for Sodium-Ion Batteries. *Adv. Energy Mater.* **2018**, *8* (22), 1800930.

(112) Qin, A.; Wu, H.; Chen, J.; Li, T.; Chen, S.; Zhang, D.; Xu, F. Constructing Hyperbranched Polymers as a Stable Elastic Framework for Copper Sulfide Nanoplates for Enhancing Sodium-Storage Performance. *Nanoscale* **2019**, *11* (15), 7188–7198.

(113) Park, J. Y.; Kim, S. J.; Chang, J. H.; Seo, H. K.; Lee, J. Y.; Yuk, J. M. Atomic Visualization of a Non-equilibrium Sodiation Pathway in Copper Sulfide. *Nat. Commun.* **2018**, *9* (1), 922.

(114) An, C.; Ni, Y.; Wang, Z.; Li, X.; Liu, X. Facile Fabrication of CuS Microflower as a Highly Durable Sodium-Ion Battery Anode. *Inorg. Chem. Front.* **2018**, *5* (5), 1045–1052.

(115) Shi, B.; Liu, W.; Zhu, K.; Xie, J. Synthesis of Flower-like Copper Sulfides Microspheres as Electrode Materials for Sodium Secondary Batteries. *Chem. Phys. Lett.* **2017**, *677*, 70–74.

(116) Li, H.; Wang, Y.; Jiang, J.; Zhang, Y.; Peng, Y.; Zhao, J. CuS Microspheres as High-Performance Anode Material for Na-Ion Batteries. *Electrochim. Acta* **2017**, *247*, 851–859.

(117) Kalimuldina, G.; Taniguchi, I. High Performance Stoichiometric Cu<sub>2</sub>S Cathode on Carbon Fiber Current Collector for Lithium Batteries. *Electrochim. Acta* **2017**, *224*, 329–336.

(118) Kalimuldina, G.; Taniguchi, I. Electrochemical Characterization of Non-Stoichiometric Cu<sub>2</sub>S<sub>x</sub> Cathode for Lithium Batteries. *J. Solid State Electrochem.* **2017**, *21* (10), 3057–3063.

(119) Kalimuldina, G.; Taniguchi, I. Sulfur-Rich CuS<sub>1+x</sub> Cathode for Lithium Batteries. *Mater. Lett.* **2021**, *282*, 128705.

(120) Qin, A.; Ji, J.; Du, R.; Tian, N.; Liao, L.; Zhang, K.; Wei, C. Hydrothermal Synthesis and Electrochemical Performance of CuS@Sisal Fiber Carbon Composite Lithium-Ion Battery Anodes. *Compos. Commun.* **2018**, *7*, 47–50.

(121) Jing, M.; Li, F.; Chen, M.; Zhang, J.; Long, F.; Jing, L.; Lv, X.; Ji, X.; Wu, T. Facile Synthetic Strategy to Uniform Cu<sub>9</sub>S<sub>5</sub> Embedded into Carbon: A Novel Anode for Sodium-Ion Batteries. *J. Alloys Compd.* **2018**, *762*, 473–479.

(122) Lou, X. W.; Archer, L. A.; Yang, Z. Hollow Micro-/Nanostructures: Synthesis and Applications. *Adv. Mater.* **2008**, *20*, 3987–4019.

(123) Sun, S.; Li, P.; Liang, S.; Yang, Z. Diversified Copper Sulfide (Cu<sub>2-x</sub>S) Micro-/Nanostructures: A Comprehensive Review on Synthesis, Modifications and Applications. *Nanoscale* **2017**, *9*, 11357–11404.

(124) Chen, Y.; Li, J.; Lei, Z.; Huo, Y.; Yang, L.; Zeng, S.; Ding, H.; Qin, Y.; Jie, Y.; Huang, F.; Li, Q.; Zhu, J.; Cao, R.; Zhang, G.; Jiao, S.; Xu, D. Hollow CuS Nanoboxes as Li-Free Cathode for High-Rate and Long-Life Lithium Metal Batteries. *Adv. Energy Mater.* **2020**, *10* (7), 1903401.

(125) Park, H.; Kwon, J.; Choi, H.; Shin, D.; Song, T.; Lou, X. W. D. Unusual Na<sup>+</sup> Ion Intercalation/Deintercalation in Metal-Rich Cu<sub>1.8</sub>S for Na-Ion Batteries. *ACS Nano* **2018**, *12* (3), 2827–2837.

(126) Fang, Y.; Guan, B. Y.; Luan, D.; Lou, X. W. D. Synthesis of CuS@CoS<sub>2</sub> Double-Shelled Nanoboxes with Enhanced Sodium Storage Properties. *Angew. Chem., Int. Ed.* **2019**, *58* (23), 7739–7743.

(127) Hosseinpour, Z.; Scarpellini, A.; Najafshirtari, S.; Marras, S.; Colombo, M.; Alemi, A.; De Volder, M.; George, C.; Lesnyak, V. Morphology-Dependent Electrochemical Properties of CuS Hierarchical Superstructures. *ChemPhysChem* **2015**, *16* (16), 3418–3424.

(128) Fang, Y.; Yu, X. Y.; Lou, X. W. D. Bullet-like Cu<sub>9</sub>S<sub>5</sub> Hollow Particles Coated with Nitrogen-Doped Carbon for Sodium-Ion Batteries. *Angew. Chem., Int. Ed.* **2019**, *58* (23), 7744–7748.

(129) Tang, J.; Ni, S.; Chen, Q.; Zhang, J.; Yang, X. CuS@Cu Freestanding Electrode via Electrochemical Corrosion for High Performance Li-Ion Batteries. *Mater. Lett.* **2017**, *201*, 13–17.

(130) Ni, S.; Lv, X.; Li, T.; Yang, X. Fabrication of Cu<sub>2</sub>S Cathode for Li-Ion Battery via a Low Temperature Dry Thermal Sulfuration Method. *Mater. Chem. Phys.* **2013**, *143* (1), 349–354.

(131) Adylkhanova, A.; Nurpeissova, A.; Adair, D.; Bakenov, Z.; Taniguchi, I.; Kalimuldina, G. Facile Synthesis of Binder-Free Three-Dimensional Cu<sub>x</sub>S Nanoflowers for Lithium Batteries. *Front. Energy Res.* **2020**, *8* (July), 1–7.

(132) Zhao, D.; Yin, M.; Feng, C.; Zhan, K.; Jiao, Q.; Li, H.; Zhao, Y. Rational Design of N-Doped CuS@C Nanowires toward High-Performance Half/Full Sodium-Ion Batteries. *ACS Sustainable Chem. Eng.* **2020**, *8* (30), 11317–11327.

(133) Park, J. Y.; Shim, Y.; Kim, Y.; Choi, Y.; Lee, H. J.; Park, J.; Wang, J. E.; Lee, Y.; Chang, J. H.; Yim, K.; Ahn, C. W.; Lee, C.-W.; Kim, D. K.; Yuk, J. M. Iron-Doped NASICON Type Sodium Ion Battery Cathode for Enhanced Sodium Storage Performance and Its Full Cell Applications. *J. Mater. Chem. A* **2020**, *8*, 20436–20445.

(134) Xiong, F.; Fan, Y.; Tan, S.; Zhou, L.; Xu, Y.; Pei, C.; An, Q.; Mai, L. Magnesium Storage Performance and Mechanism of CuS Cathode. *Nano Energy* **2018**, *47* (March), 210–216.